J. Fluid Mech. (1989), *vol.* 209, *pp.* 463–499
Printed in Great Britain

Experiments on mixing due to chaotic advection in a cavity

By C. W. LEONG AND J. M. OTTINO
Department of Chemical Engineering, University of Massachusetts, Amherst, MA 01003, USA

(Received 16 August 1988 and in revised form 10 March 1989)

Chaotic mixing of fluids in slow flows is ubiquitous but incompletely understood. However, relatively simple experiments provide a wealth of information regarding mixing mechanisms and indicate the need for complementary theoretical developments in dynamical systems. In this work we present a versatile cavity flow apparatus, capable of producing a variety of two-dimensional velocity fields, and use it to conduct a detailed experimental study of mixing in low-Reynolds-number flows. Since the goal is detailed understanding, only two time-periodic co-rotating flows induced by wall motions are considered: one continuous and the other discontinuous. Both types of flows produce exponential growth of intermaterial area, as expected from chaotic flows, and a mixture of islands and chaotic regions. A procedure for identifying periodic points and determining their movements is presented as well as how to make meaningful comparisons between periodic flows. We observe that periodic points move very much as a planetary system; planets (hyperbolic points) have moons (elliptic points) with twice the period of the planets; furthermore the spatial arrangement of periodic points becomes symmetric at regular time intervals. Detailed analyses reveal complex behaviour: birth, bifurcation, and collapse of islands; formation and periodic motion of coherent structures, such as islands and large-scale folds. However, the richness and complexity of the results obtained indicate that these two-dimensional time-periodic systems are far from completely understood and that other wall motions might deserve a similar level of scrutiny.

1. Introduction

Mixing of viscous fluids without molecular diffusion is ubiquitous in nature and industry. It is relevant to problems ranging from geophysics to the processing of polymers; however, various aspects are still not understood. In fact, with the exception of a handful of articles on polymer processing and earth sciences, the topic has received disproportionately little attention and only a few works have addressed the problem from an experimental viewpoint (for references in the context of polymer processing see Middleman 1977; Ottino & Chella 1983, for the role of mixing in earth sciences, see Allègre & Turcotte 1986 and Weijermars 1988). In this article we present a detailed experimental analysis of the mixing structures produced in a class of two-dimensional time-periodic flows capable of producing chaotic advection.†

The primary objective of this work is to develop techniques for the analysis of mixing in chaotic flows without an exact knowledge of the velocity field.

† A description of applications, as well as a short preview of the results corresponding to this system as well as others, was published recently (Ottino *et al.* 1988). Background material, as well as analytical and computational examples of chaotic mixing in various systems are presented in Ottino (1989*a*).

Conventional computational and analytical studies (see table 7.1 in Ottino 1989*a*) necessitate an analytical solution for the velocity field which is unavailable in most cases of practical interest. Other systems, such as the flow between eccentric cylinders can be analysed also in terms of computations (Aref & Balachandar 1986; Chaiken *et al.* 1986; Swanson & Ottino 1990). However, as has been pointed out, there are inherent limitations to computational studies, and computational, analytical, and experimental studies play complementary roles in the analysis of mixing (Ottino *et al.* 1988). Rather 'simple' mixing flows, such as those corresponding to the experiments reported here can take 10^2 years of computational time in a megaflop machine (Franjione & Ottino 1987). Also, an investigation of chaotic mixing in two-dimensional time-periodic flows provides a transparent visual analogue for chaos in area-preserving maps and Hamiltonian systems, some of the oldest and most established systems to be analysed in the context of what is now grouped under the heading of dynamical systems (see Ottino 1989*a*). Indeed, experimental studies can be regarded as an analogue of the usual discrete computational investigations and in several instances provide a finer resolution.

In this article we seek an understanding of chaotic mixing based upon the observation of the resulting macroscopic structures, and their variation and bifurcation with the governing parameter of the flow. The structures under consideration will be those that are delineated rather quickly and the main parameter will be the period of the motion of the walls. The reader should note that there are two main aspects that distinguish the present kind of studies from more conventional studies in dynamical systems and chaos. The first aspect is that we are interested mostly in rate processes, i.e. rapid mixing, rather than asymptotic structures and long-time behaviour, as is for example, a Poincaré section. The second aspect is that the perturbations from integrability are large, since this is what happens (roughly) when the best mixing occurs. These aspects, coupled with the absence of an analytical description of the flow, preclude analyses based on perturbative techniques (i.e. the standard Melnikov's method).

2. Experimental

The model system chosen in this work is a substantially improved version of the cavity flow system introduced by Chien, Rising & Ottino (1986). The flow system, in general, consists of two moving walls and two static walls immersed in a fluid bath, as shown in figure 1. The walls motions are computer controlled, such that different types of wall velocity functions can be produced with relative ease. Depending on the motion of the walls, a variety of two-dimensional flows can be generated but only a few are considered here. To study the mixing process, we follow the deformation of a blob of a line of tracer, which is injected in the fluid.

2.1. *Experimental apparatus*

The principal objective is to design an apparatus capable of generating a variety of two-dimensional flows and geometrical configurations. However, only one cavity configuration and two types of flows are explored in this paper; it will be apparent that other operating conditions deserve a similar study. A schematic view of the apparatus is shown in figure 1. The mixing experiments are conducted in a flow region confined between the belts, acting as moving walls, and the static walls (figure 1*a*); (x, y)-coordinates are chosen such that the origin $(0, 0)$ is at the centre of the cavity, z is the direction normal to the (x, y)-plane of the flow. The area of the cavity

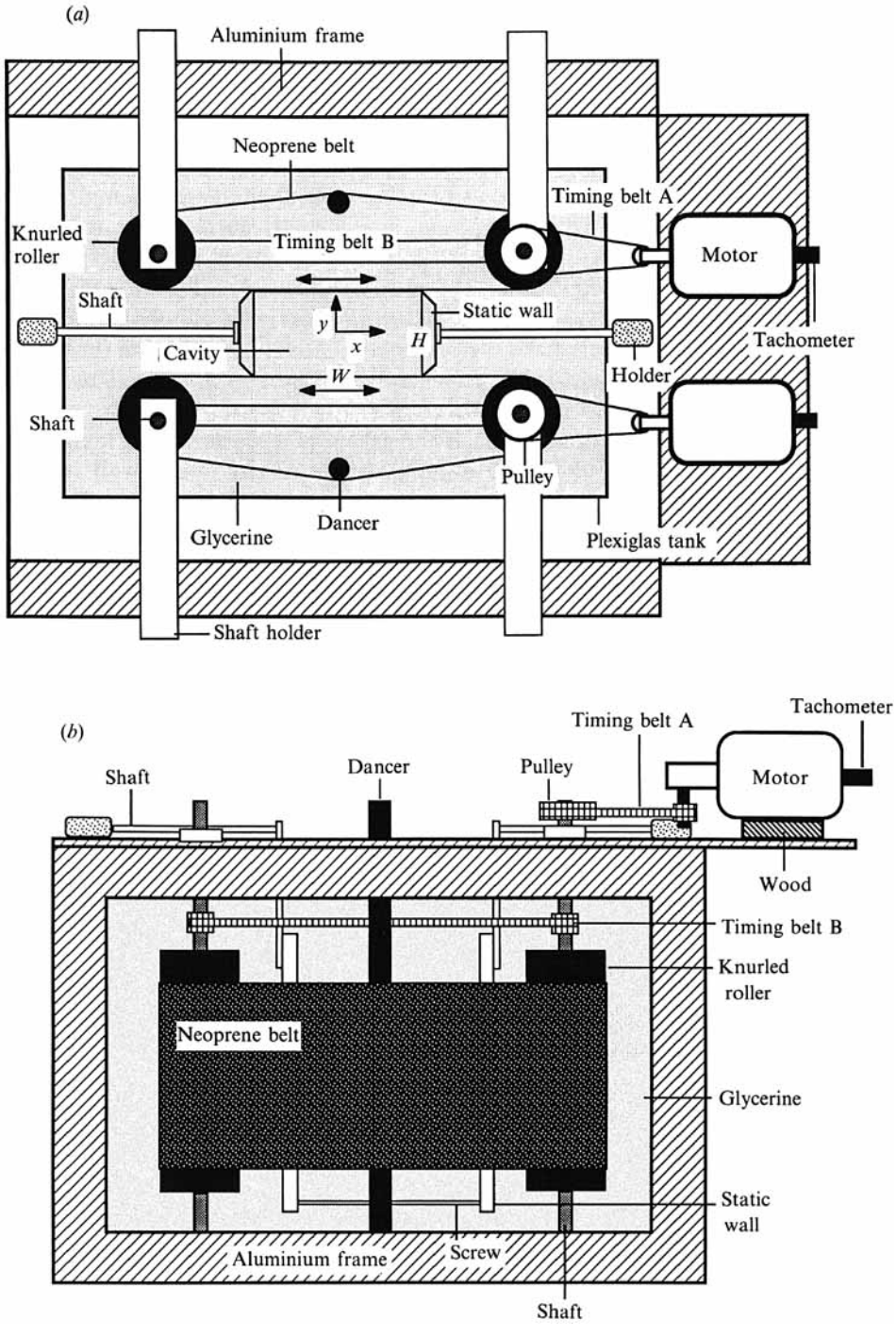

FIGURE 1. Schematic of the cavity flow apparatus: (*a*) top view; (*b*) side view. The dimensions of the cavity itself are $H = 6.2$ cm and $W = 10.35$ cm.

can be adjusted up to a maximum of 167.4 cm^2. In the experiments presented here, the aspect ratio W/H is 1.67 with $W = 10.35$ cm and $H = 6.2$ cm. We focus exclusively on a rectangular cavity although other shapes, such as a trapezoidal cavity, can be implemented by changing the positions of the belts and the baffles. The apparatus mainly consists of three parts: the belt unit, the static wall unit, and a supporting structure.

There are two belt units, each consisting of two knurled rollers (aluminium, 7.62 cm diameter, 25.4 cm long), a neoprene belt (20.3 cm deep, 1.6 mm thick), and a DC shunt-wound motor (B & B Motors, model NSH-54RL, gear reduction ratio 1:300); each motor has a built-in tachometer (B & B Motors, model SB-7427A-7) that generates 2.6 v.d.c. per 1000 r.p.m. The motor drives one roller directly with timing belt A (figure 1*b*). The second roller is driven indirectly by the first roller via timing belt B. The rollers then drive the neoprene belt. Additional tension on the neoprene belt is supplied by an adjustable dancer. The dancer is also used to prevent the creeping of the belt due to friction drive of the rollers and the belt.

There are two static wall units, each consisting of a static wall (Plexiglas, 30.5 cm deep), a shaft, and a holder. The angular edges of the static wall minimize the contact with the moving belt. The shaft is attached to the static wall, which slides easily through the holder thus allowing the cavity aspect ratio and geometry to be easily modified. The holder is tightened to hold the wall in a fixed position. In addition, the bottoms of the walls are connected to a screw to ensure that they are fixed.

The supporting structure consists of a Plexiglas tank (40.7 cm deep) and an aluminium frame. The Plexiglas tank houses all the units and is filled with glycerine (96% pure, viscosity 7.5 poise, density 1.25 g/ml) up to 35 cm deep. The aluminium frame reinforces the Plexiglas tank and serves to hold the two motors and the holders.

2.2. *Computer control system*

The computer control system (see figure 2*a*) has three functions: (i) to control the speed of each motor (and hence the speed of each moving wall); (ii) to control the direction of rotation of each motor (and hence the direction of movement each wall); and (iii) to control the motor drive of the camera. These functions are accomplished using a microcomputer with a multi-channel digital/analog (D/A) interface. A computer program individually controls the analogue output on each of three channels (corresponding to the functions); these signals are then conditioned, as necessary, to provide the desired function.

The Apple IIe computer system and the D/A interface (Mountain Computer 8-bit D/A board, 16 analog output channels, ± 5 v.d.c. output, 9 μs conversion time) are controlled by a program written in BASIC. The program ouputs a number to the appropriate channel on the D/A board to determine the output on that channel. For the motor-direction control channel, and the camera control channel, this is merely on or off (0 or 3 v.d.c.); for the motor-speed control channel, it is a stepwise variable (0–3 v.d.c.). Event timing (length of time for the walls to move, when to change directions, etc.) is controlled by the repetition number of a do-loop in the program. To ensure accuracy, the wall speed was calibrated with the digital output, using a linear least-squares technique (accurate to ± 0.01 cm/s). Similarly, the timing was calibrated with the repetition number of the do-loop (accurate to ± 1 ms).

The speed of the motors is proportional to their input voltage (maximum speed at 110 v.d.c.). The analog output from the computer goes to a signal isolator (Penta KB

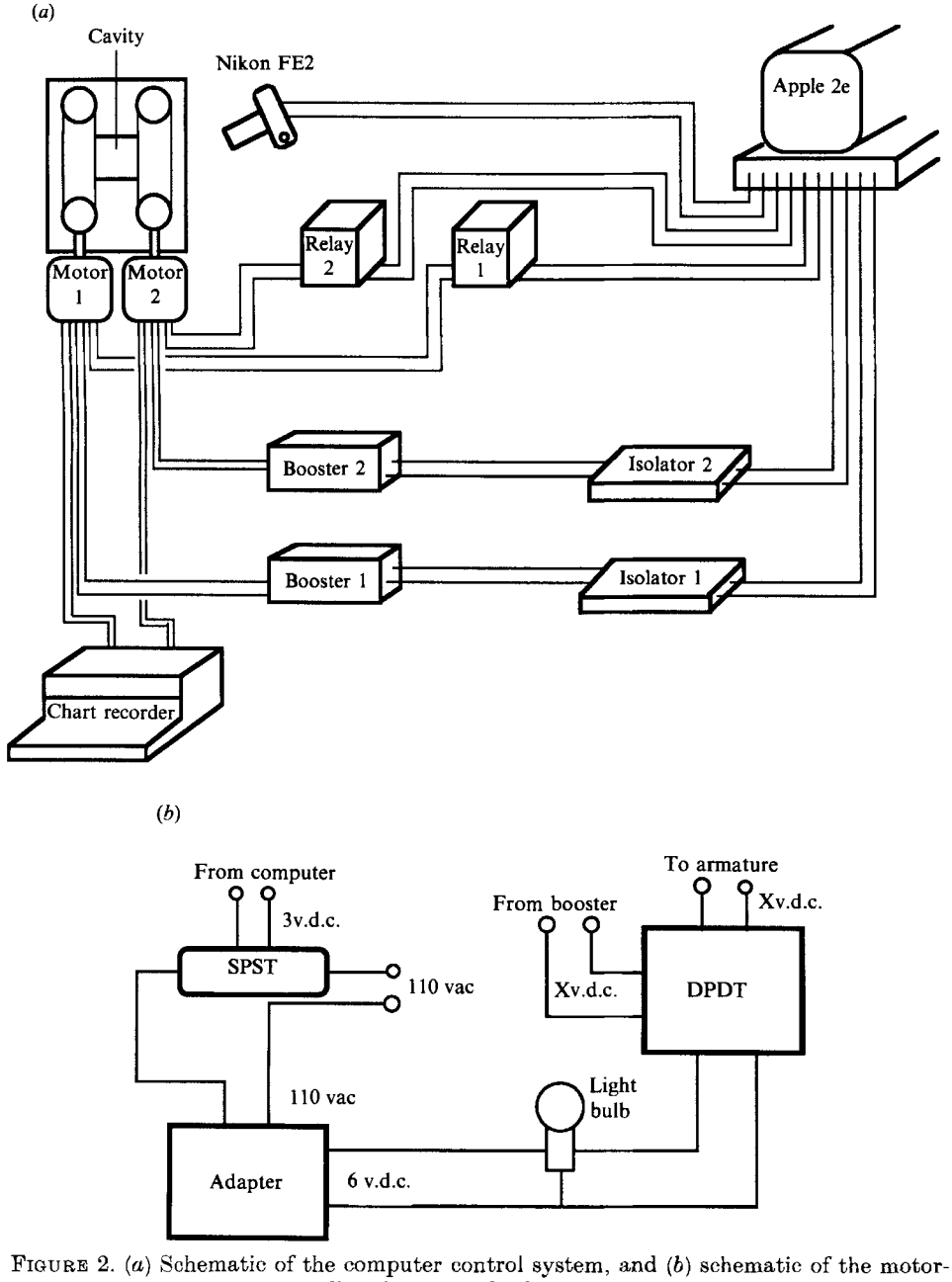

FIGURE 2. (*a*) Schematic of the computer control system, and (*b*) schematic of the motor-direction control relay circuit.

Power, model KBSI-240D) to protect the D/A interface; the isolated signal is sent to a voltage 'booster' (B & B Motors, model SH 102), and the boosted signal drives the motors. The working range of the analog output is 0–3 v.d.c., which corresponds to 0–110 v.d.c. from the booster. The motor changes its direction of rotation when the polarity of its armature is reversed. This is accomplished with a relay system (see figure 2*b*), consisting of a single-pole-single-throw (SPST) relay (Radio Shack, 275-232), a double-pole-double-throw (DPDT) relay (Newark Electronics, 21F1080),

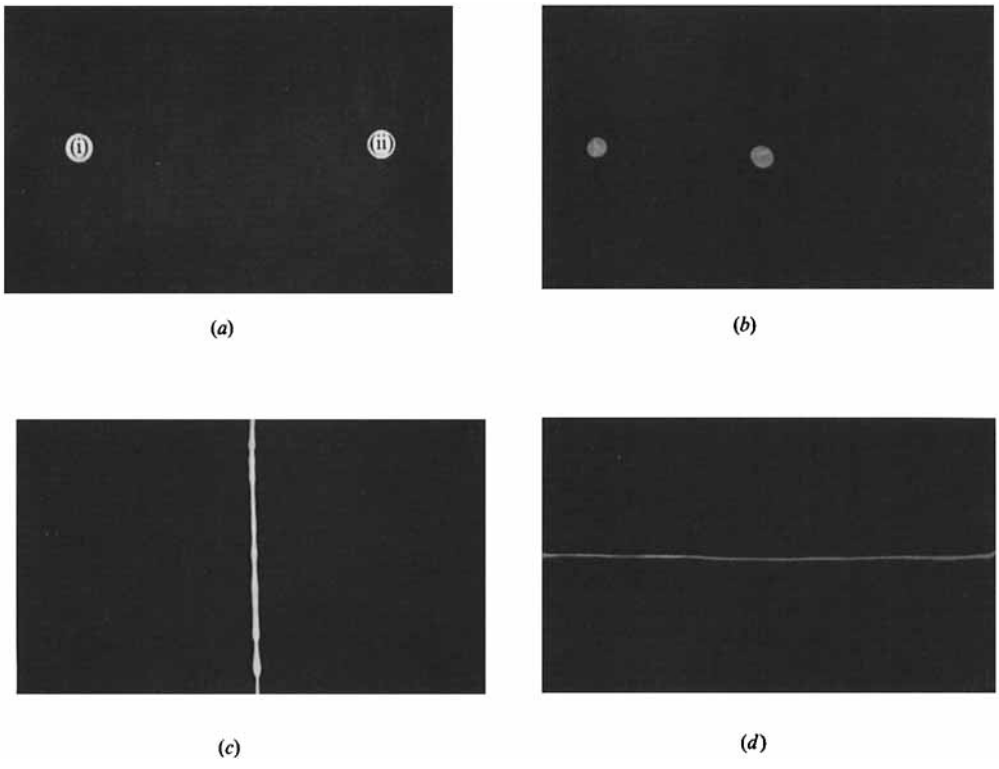

FIGURE 3. Various sets of initial conditions used for conducting blob and line deformation experiments. The tracer is injected approximately 5–10 mm underneath the free surface. In (*a*) a blob, (i) or (ii), is located along the x-axis approximately 1.27 cm away from the left (or right) static wall; in (*b*) one blob is located at the centre of the cavity, while the other is located 1.27 cm away from the left static wall and along the x-axis; in (*c*) the initial condition is a line of dye along the y-axis; in (*d*) the initial condition is a line of dye along the x-axis.

and a 6 v.d.c. adapter (Radio Shack, 273-1651). The computer sends an analog signal to close the gate of the SPST relay, allowing 110 V to flow from the main power supply to the adapter. The adapter then outputs 6 v.d.c., closing the gate of the DPDT relay, which switches the armature poles. A 6 v.d.c. light bulb is connected parallel with the line from the adapter to the DPDT relay, to give a visual indication of which direction the motors are turning. The camera shutter is activated (causing a picture to be taken), and the film is advanced, when the motor drive circuit is closed. This is accomplished with a SPST relay connecting the motor drive circuit to the analog output.

2.3. *Flow visualization*

To study the mixing process, we follow the deformation of a blob or a line of tracer. The tracer is injected with a syringe, roughly 5–10 mm underneath the free surface of the fluid, at one or more carefully preselected locations. The tracer, a blob or a line, is then allowed to stretch and fold with the bulk fluid for a specific amount of time; all the initial conditions used in our experiments are shown in figure 3. In principle we can conduct experiments with a variety of tracers, active or passive (Ottino 1989*a*). In our studies, we choose to use a passive tracer which is a fluorescent dye made up of fluorescent power (Cole-Palmer, type J-295) dissolved in glycerine.

The diffusion coefficient of the dye is estimated to be 10^{-8} cm^2/s and its density is relatively close to that of glycerine. In fact, the dye solution can be suspended in glycerine for a few days without sinking to the bottom or rising to the surface. The dye is excited by two sets of long-wave 365 nm UV lights (Fisher, model XX-15N) that are hung directly above the cavity along the x-direction. When excited, the dye is coloured red, while, owing to some amount of UV absorption, the glycerine appears light blue.

A Nikon FE2 camera with a Nikkor micro f/4.0 105 mm lens is mounted above and perpendicular to the flow field. The working distance is between 43 and 55 cm. Kodak T-Max 100 ASA film is used with an f-stop of 4.0 and an exposure time of 0.5 or 1 s. A yellow filter (Quantaray, Y2) is added to enhance the contrast between the glycerine and the dye, and to reduce the UV reflections from the free-surface. The entire mixing experiment (evolution of the initial conditions) is recorded on video tape, using a 512 × 512 resolution B/W TV camera (Dage MTI-65), a Panasonic VHS recorder (model AG-6300), a FOR.A video timer (model VTG-55), and a Sony Trinitron monitor (model PVM-1910Q).

2.4. *Time-periodic co-rotational flows and experimental conditions*

We consider two types of time-periodic wall motions (figure 4*a*, *b*); a discontinuous flow and a sinusoidal flow. Both flows are co-rotational; the word 'co-rotational' is used to designate that the top and bottom walls move in opposite directions; throughout this paper, the top wall moves first, unless otherwise indicated, from left to right and the bottom wall moves second from right to left. In the discontinuous co-rotational flow, the top wall moves for half a period $\frac{1}{2}T$ and the bottom wall also moves for half a period $\frac{1}{2}T$; both walls move at 1.9 cm/s and there is a 5 s pause between each half-period. The sinusoidal co-rotational flow is of the form

$$v_{\text{top}} = U_{\text{top}} \sin^2\left(\frac{\pi t}{T_{\text{top}}} + \alpha\right), \tag{2.1}$$

$$v_{\text{bot}} = U_{\text{bot}} \sin^2\left(\frac{\pi t}{T_{\text{bot}}}\right), \tag{2.2}$$

where $|U_{\text{top}}| = |U_{\text{bot}}| = U = 2.69$ cm/s, $T_{\text{top}} = T_{\text{bot}} = T$. This flow is referred to as the sinusoidal flow. There are two parameters in this flow: the period T and the phase angle α. We consider the period T as the main governing parameter; the phase angle α will be either $\frac{1}{2}\pi$, throughout most of the work, or $\frac{1}{4}\pi$, as in §4.2.2. The velocity U and the period T are selected such that both inertial effects and dye diffusion are negligible. The magnitude of the inertial effects is given by the Reynolds number and the Strouhal number

$$Re = \frac{U}{\nu}\left(\frac{H^2}{W}\right), \quad Sr = \left(\frac{H^2}{W}\right)\left(\frac{1}{TU}\right),$$

where H and W are the height and width of the cavity, and ν is the kinematic viscosity. In our experiments, the maximum wall speed is 3.5 cm/s and the operating range of Re, using glycerine at 25 °C, is 0.5–1.7. In all the experiments, Sr is 0.10–0.20.

The operating conditions are determined by the following considerations. In order to minimize diffusion effects the experiments should be conducted quickly; however,

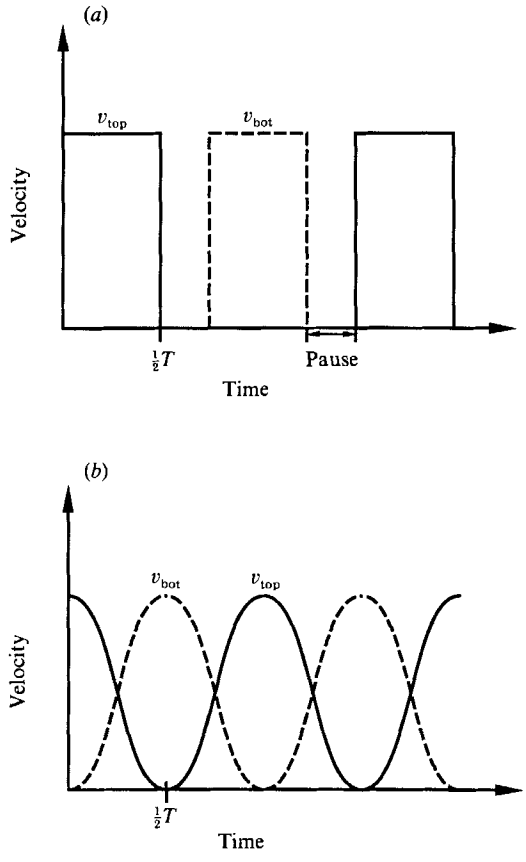

FIGURE 4. Wall motions corresponding to: (*a*) the discontinuous flow and (*b*) the sinusoidal flow used in the experiments; v_{top} and v_{bot} are the top and bottom wall velocities, respectively, and T is the period. Note that in both cases the top wall moves first for $\frac{1}{2}T$ to exploit the symmetries of the flow.

this might result in inertial effects and secondary flows. Conversely, vanishingly small Re necessitate long experiments to produce noticeable blob or line stretching and, hence, diffusion becomes important. We found that the best compromise corresponds to $Re = O(1)$. The timescale for inertial (transient) effects using glycerine as the working fluid is of order 10^{-2} s, which is very small compared with the period T (order 10^1–10^2 s).

The importance of the inertial effects can be checked experimentally by stretching an initial condition in discontinuous and continuous modes for a given amount of wall displacement and then reversing the wall motion. Typically, we found these effects to be negligible. As a test, we conducted two experiments with $Re = 1.7$, a duration of 5 min, and a blob located at the centre of the cavity: first, a continuous uninterrupted wall motion, and second, a sequence of stopping and instantly restarting the motion five times. Both modes of operation showed nearly identical final results. More importantly, both showed kinematical reversibility (i.e. the deformed blob returns to its initial location). If inertial effects were important, the flows would not be kinematically reversible.

As long as the creeping-flow assumption holds, the distance travelled by the

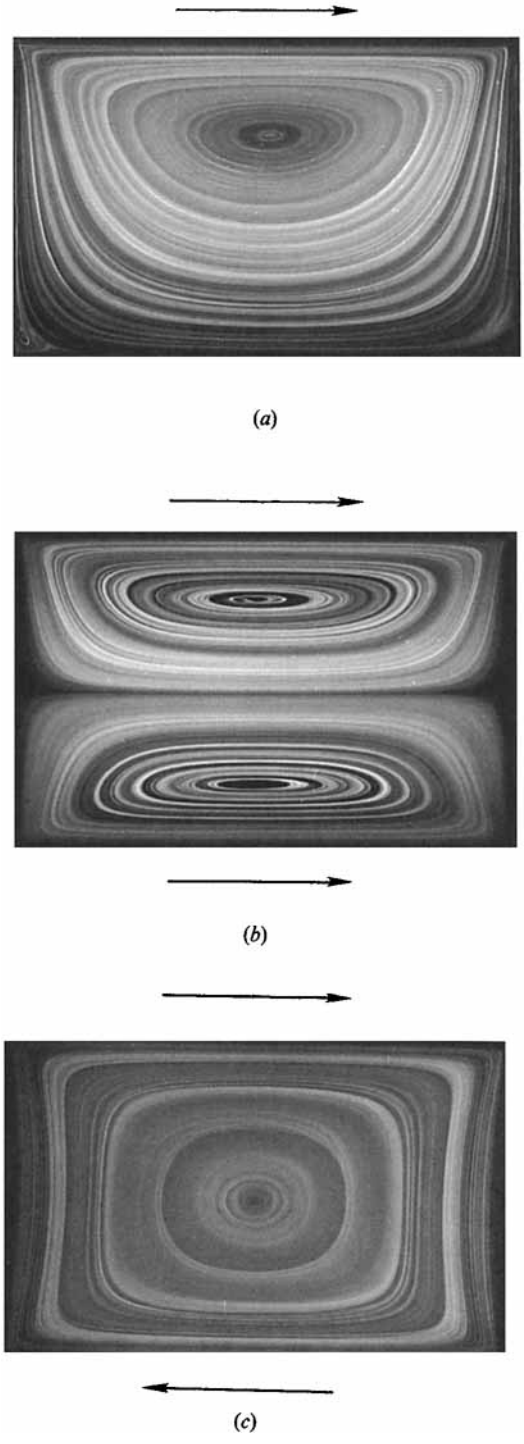

FIGURE 5. Steady-state (or instantaneous) streamlines corresponding to: (*a*) top wall moving; (*b*) two walls moving in the same direction; (*c*) two walls moving in opposite directions; $v_{top} = 1.58$ cm/s, $v_{bot} = 1.58$ cm/s ($Re = 1.0$). In all cases the initial condition is a line of dye injected along the y-axis (see figure 3*c*).

moving walls is the most suitable parameter for quantification of the experiments.† During the time T (one period) the walls move a distance

$$d_{\text{top}} = \int_0^T v_{\text{top}}(t)\,\mathrm{d}t, \quad d_{\text{bot}} = \int_0^T v_{\text{bot}}(t)\,\mathrm{d}t, \tag{2.3}$$

$$D = \frac{|d_{\text{top}}| + |d_{\text{bot}}|}{W}, \tag{2.4}$$

where d_{top} and d_{bot} are the displacements of the top wall and bottom wall respectively, and D is the dimensionless wall displacement per period. In addition, we define a dimensionless total wall displacement $N_d = DP$, which is a measure of the distance travelled by the walls in width units and is proportional to the total number of periods (P).

2.5. *Streamlines*

There are three basic types of steady flows: (i) flows with one wall moving, (ii) flows with two walls moving in the same direction, and (iii) flows with two walls moving in the opposite direction; we study all three cases, under the restriction that both walls move at the same speed. Within the creeping-flow assumption, the streamline portraits are independent of the actual speed of the walls. Excellent approximations to the streamlines can be obtained from long-time line deformation experiments: initially, a line of dye is injected 5 mm underneath the free surface and in the centre of the cavity along the y-axis (figure 3*c*). Then the line is allowed to stretch for 20 min, with a wall speed of 1.58 cm/s. At this point the dye filaments lie almost tangential to the steady streamlines (see figure 7(*a–c*), which corresponds to shorter times; the stretching time should be selected carefully; a much longer time, say 60 min, results in poor resolution). Next, while the flow is still in motion, a long-time exposure picture is taken. The exposure time is approximately 2 min with an f-stop of 4.0 and a red-filter (Quantaray, R2) using Kodak T-Max 100 ASA film. Streamlines portraits obtained using this method are shown in figure 5(*a–c*).

A similar type of experiment was used to check the two-dimensionality of the flow. An indication of two-dimensionality, or lack thereof, can be obtained in the following way: two of the initial conditions are placed at different depths, one on top of the other. Since the flow is chaotic, small errors are magnified exponentially fast, and any deviation from two-dimensionality results in crossing of striations. We did not observe any crossing even at the highest Reynolds numbers encountered in this work. Note also that it is not necessary to check two-dimensionality in all experiments. Indeed, if the flow is not two-dimensional, the stretching and folding experiments conducted using a single blob will also show crossing of striations. However, as can be observed in the many photographs shown in this paper, the striations do not show any significant crossing, and the flow is indeed two-dimensional.

3. Definitions of terms used in the interpretation of the results

Here we collect various definitions used in the interpretation of the experimental results. The most frequently used terms we shall encounter are *periodic points* (such as elliptic and hyperbolic periodic points); *islands*; *bifurcations*, *birth*, and *collapse* of

† It should be noted that time is only a parameter and does not appear explicitly in a mathematical description of the system. That is, if we run one experiment, and then a second one at twice the speed but using half the time, each will produce identical results. We have verified this fact experimentally (both experiments are run under creeping-flow conditions).

islands; and *coherent structures*. However, in a rather loose sense, we shall speak also of the *shape* or *size* of an island, even though these terms are not defined precisely from a mathematical viewpoint.

A program for the investigation of chaotic fluid flows starts with the Eulerian velocity field $\boldsymbol{v}(\boldsymbol{x},t)$ (e.g. obtained as a solution of the Navier–Stokes equations with $\boldsymbol{\nabla}\cdot\boldsymbol{v}=0$). The pathline of a fluid particle initially located at $\boldsymbol{x}=\boldsymbol{x}_0$ corresponds to the solution of

$$\frac{\mathrm{d}\boldsymbol{x}}{\mathrm{d}t}=\boldsymbol{v}(\boldsymbol{x},t), \tag{3.1}$$

with the initial condition $\boldsymbol{x}=\boldsymbol{x}_0$. The solution of (3.1) for all $\boldsymbol{x}_0$ belonging to the flow domain is called the flow or motion and is denoted as

$$\boldsymbol{x}=\phi_t(\boldsymbol{x}_0) \quad \text{with} \quad \boldsymbol{x}_0=\phi_{t=0}(\boldsymbol{x}_0), \tag{3.2}$$

signifying that the fluid particle initially located at $\boldsymbol{x}_0$ will be found at position $\boldsymbol{x}$ at time t. In two dimensions $\boldsymbol{v}=(v_x,v_y)$, $\boldsymbol{x}=(x,y)$, and the flow $\boldsymbol{x}=\phi_t(\boldsymbol{x}_0)$ is an area-preserving transformation. In particular the system (3.1) has a Hamiltonian structure:

$$\frac{\mathrm{d}x}{\mathrm{d}t}=\frac{\partial\psi}{\partial y}, \quad \frac{\mathrm{d}y}{\mathrm{d}t}=-\frac{\partial\psi}{\partial x}, \tag{3.3}$$

where ψ is the stream function (Aref 1984). It is possible to assert that if the velocity field is steady, i.e. ψ is independent of time, the velocity field is integrable and the system cannot be chaotic. On the other hand, if the velocity field, or equivalently ψ, is time-periodic, the phase space of the system has one additional dimension, and there is a good chance that the system will be chaotic. Indeed such systems appear to be common in practice and a few have been studied experimentally (Chien *et al.* 1986; Chaiken *et al.* 1986; Ottino *et al.* 1988). As we shall see, however, the fact that the system is Hamiltonian is not particularly useful in the interpretation of the results.

In the special case of a time-periodic velocity field, $\boldsymbol{v}(\boldsymbol{x},t)=\boldsymbol{v}(\boldsymbol{x},t+T)$, the flow (3.2) can be reduced to a mapping

$$\boldsymbol{x}_{n+1}=\phi_T(\boldsymbol{x}_n), \tag{3.4}$$

where we identify the position of $\boldsymbol{x}_0$ at time $t=T$ as $\boldsymbol{x}_1$, at time $t=2T$ as $\boldsymbol{x}_2$, and so on. Since the velocity field is bounded, some fluid particles return exactly to their original positions whereas others pass arbitrarily close to their starting points. For the system (3.4), if a designated particle at $t=0$ returns exactly to its initial position after one period, i.e. $t=T$, but not before, then the initial location corresponds to a periodic point of period one; if it returns after two periods, $t=2T$, but not before then, the point is of period two, and so on.

Much of the understanding of the complex behaviour of chaotic systems resides in the character and structure of the periodic points in the flow. The periodic points can be classified as hyperbolic, elliptic, or parabolic, according to the deformation of the fluid in the neighbourhood of the periodic point (the parabolic case being degenerate). The character of the point is given by the eigenvalues of the linearized mapping in the neighbourhood of the point. For a hyperbolic point, the two eigenvalues are real, while for an elliptic point, the two eigenvalues are complex conjugates of magnitude one. The hyperbolic points have associated invariant regions of inflow and outflow called the stable and unstable manifolds (a very simple introduction to periodic points and their associated manifolds in the context of mixing appears in Ottino

1989*b*). If the stable and unstable manifolds belonging to a hyperbolic periodic point intersect transversely, they form what is called a transverse *homoclinic* intersection. On the other hand, if the stable and unstable manifolds belonging to two different hyperbolic periodic points intersect transversely, they form a transverse *heteroclinic* intersection (for more precise mathematical definitions, see Guckenheimer & Holmes 1983).

A system can be classified as chaotic if it satisfies any of the following criteria: (i) the flow produces either transverse homoclinic or transverse heteroclinic intersections, (ii) the flow has a positive Liapunov exponent, or (iii) the flow is able to stretch and fold material in such a way that it produces what is called a horseshoe map (strictly speaking, these definitions are not equivalent, their interrelation is discussed by Doherty & Ottino 1988). The flows analysed in this work can be classified as chaotic according to definition (iii), as indicated by Chien *et al.* (1986). Furthermore, in §4.1, we present evidence that they also satisfy definition (ii).

Our task is to identify some of these structures in a fluid flow. However, how can a point be labelled as either hyperbolic or elliptic in an actual experiment? The first step is to show that the point is indeed periodic. Then, the order of the point is determined by the number of periods it takes the point to return to the same location. Theory, specifically the KAM theorem (see, for example Guckenheimer & Holmes 1983) indicates that the elliptic points are surrounded by invariant curves or islands, which translate and rotate, conserving their identity. Islands do not exchange matter with the rest of the fluid and, therefore, represent an obstacle to efficient mixing. Experimentally, if the point is elliptic, it usually appears as a hole or an island (not dye-filled) with a finite area, unless the dye was located in the neighbourhood of the point at the very beginning of the experiment. It should be clear that the central elliptic point of an island cannot be located exactly and its position can only be estimated within experimental error. Usually, the central elliptic point is located close to the centre of the island. We have observed that the flow within islands is mostly rotational, the stretching is linear, and the rates of stretching are usually much slower than in the chaotic regions of the flow.† In a typical experiment, the shape of a large island is delineated quickly in just a few periods, as little as four or five, and achieves some asymptotic shape as the number of periods is increased. The order of an island is defined as the number of periods the island takes to return to the same location. Indeed the most readily observable features in our experiments are islands and large-scale structures, such as folds. Islands and large-scale folds are coherent, i.e. they can be labelled and followed in space and time. If a periodic point is not elliptic than it follows that it must be hyperbolic. To verify that the point is actually hyperbolic, we examine the stretching of the surrounding structure formed during the mixing process. Material is compressed in one direction while stretched in another. If we place a blob on top of a hyperbolic point, the blob traces the structure of the unstable manifold. The typical structures located in the neighbourhood of a hyperbolic point are shown in figure 6.

The application of the above definitions is not trivial, and a complete experimental investigation can be quite tedious. For example, in order to justify that a point is time-periodic, first a series of pictures is taken in between periods so that the evolution of the structures can be followed precisely. The analysis is, in general, made

† Similar results have been observed in both computer simulations and experiments in the flow between two eccentric cylinders (Swanson & Ottino 1990).

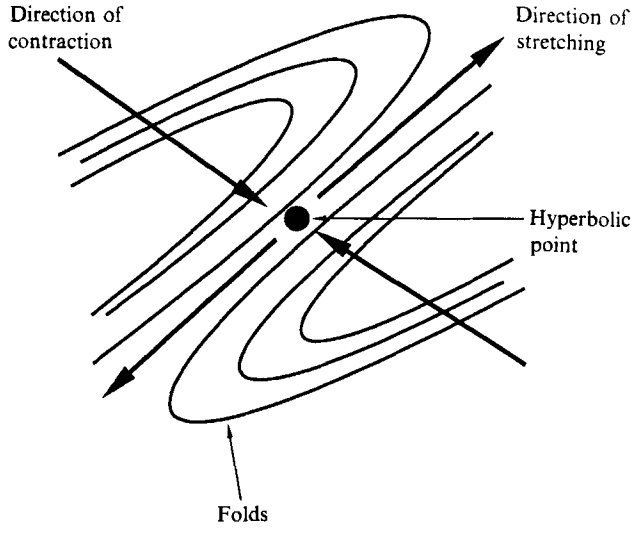

FIGURE 6. Sketch of the structure formed by a blob deformation experiment in the neighbourhood of a hyperbolic periodic point.

easier by asymptotic structures which are established rather quickly (indeed the term attractor, even though it is inappropriate for area-preserving systems, comes to mind). The number of pictures required is determined by the suspected order of the point under investigation. Our approach is to initially record the entire mixing experiment on video tape, and then review the experiment enough times as to be able to identify target points. Based on this information, we decide on the number of pictures needed. A rule of thumb is to take pictures at $\frac{1}{4}$ period intervals; for example, identifying a period-4 point needs 17 pictures to show that the point actually returns to the initial location after 4 periods. Obviously, these pictures can also be used to identify the character of the point under analysis.

The bifurcation of an island is defined as an island breaking up into two or more islands when a governing parameter is varied (in our case, the period T or displacement D). Usually, the bifurcation occurs when the central elliptic point of the island changes to hyperbolic. Conversely, the hyperbolic point can change to elliptic, thus forming an island. In some cases, a change in the governing parameter causes the island to collapse completely, that is, within experimental resolution, the island disappears and no new islands are born.

4. Chaotic mixing

Here we present experimental results of chaotic mixing produced by the discontinuous and sinusoidal flows. We begin by presenting a quantitative technique used to measure the stretching rates; it will be apparent that new ways of quantifying mixing are needed, especially for chaotic mixing. We then proceed to discuss experiments focusing on the overall changes in mixing behaviour as a function of the dimensionless wall displacement D. Finally, we choose two specific cases and use them to illustrate and discuss in detail the bifurcation, birth, and collapse of islands, and the structure of periodic points and coherent structures.

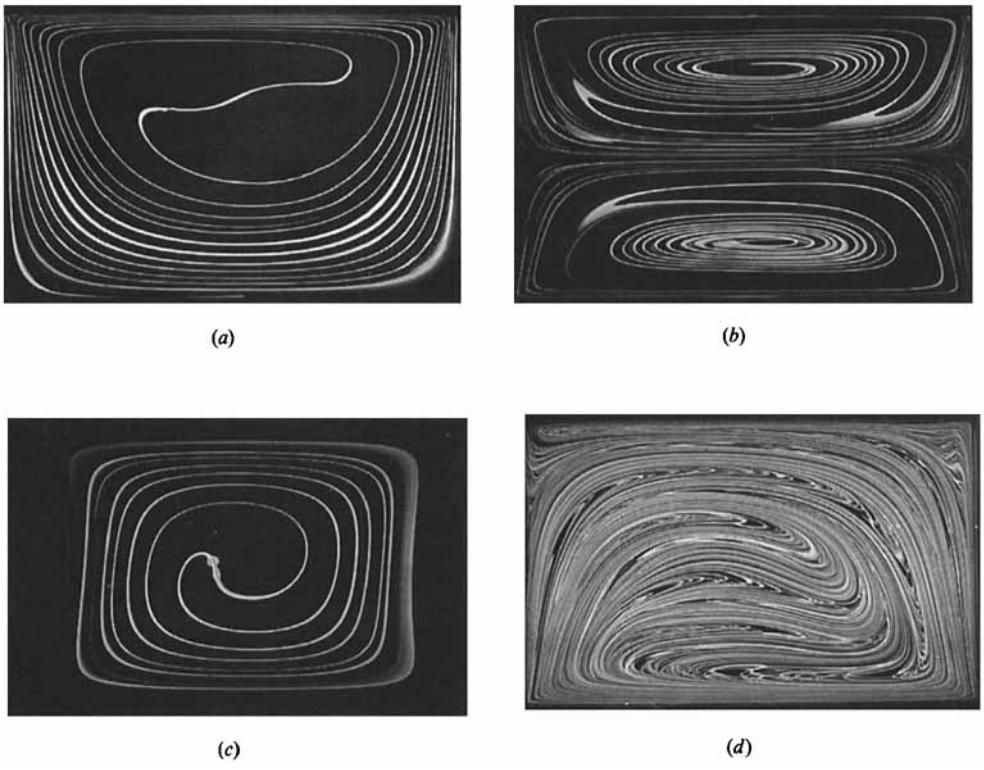

FIGURE 7. Comparison of mixing in steady and chaotic flows. The initial condition is a line of fluorescent dye injected 5 mm below the free surface at the centre of the cavity, along the y-axis (see figure 3c). The three steady flows (a–c) correspond to figure 5(a–c), while, the chaotic flow (d) corresponds to the discontinuous corotational flow ($D = 12.85$). The top and bottom wall velocity is 1.9 cm/s. The total mixing time is 5 min for the steady flows with displacements N_d of (a) 55, (b) 110, (c) 110. The total mixing time in the chaotic flow is 4 min 40 s (a total of 4 periods) with $N_d = 51.4$. It is apparent that the chaotic flow mixes much better than the steady flows in terms of stretching and dispersion.

4.1. *Measurement of stretching rate*

In mixing studies, stretching rates are commonly used to determine the effectiveness of a flow to generate good mixing. It is now known that steady bounded flows can generate at best a linear stretching rate, while time-periodic flows have a good chance of generating exponential stretching rates, at least in some regions of the flow. Exponential stretching is important since it implies exponential generation of material interface. This in turn enhances rate of mass transfer between the fluids, and has several practical consequences.

The main reason that steady two-dimensional flows can only provide linear stretching is that material lines align with the streamlines after a short time (see Ch. 4 in Ottino 1989a). Examples of this behaviour are shown in figure 7(a–c). Figure 3(c) shows the initial condition for all the cases, figure 7(a) corresponds to moving the top wall, figure 7(b) to moving top and bottom walls in the same direction, figure 7(c) to moving top and bottom walls in opposite directions. As shown in the photographs, the dye line aligns with the steady streamlines and the mixing is poor. A dramatic contrast to this situation is provided by time-periodic operation of the cavity walls; figure 7(d) shows the result of a discontinuous corotational flow for a total of 4

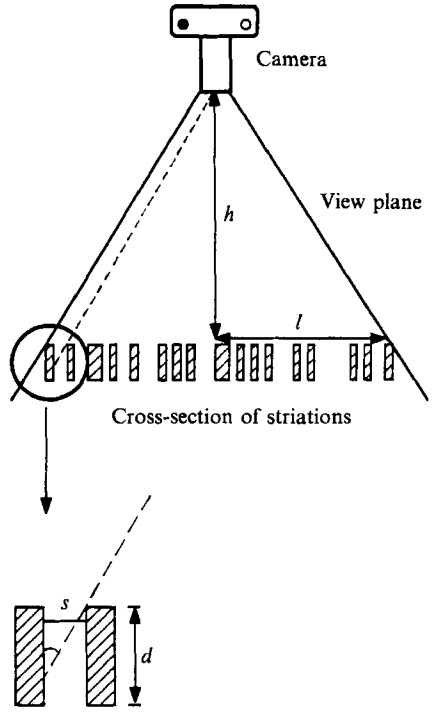

FIGURE 8. Schematic of the effects produced by the height of the striations. The striations away from the focal point appear thicker than they actually are since the camera sees the lateral area of the striations. It is estimated that two striations closer than 10 μm are indistinguishable to the camera in our set-up.

periods. Clearly, the time-periodic operation is substantially more effective in terms of mixing than the steady flows.

In order to determine the effectiveness of mixing by the time-periodic and steady flows, we utilize image analysis. The main quantity of interest is the intermaterial area (perimeter) between the dye and the clear fluid as a function of time. We expect the continual stretching of the dye filaments to keep the dye concentration high and the diffusional penetration distance small; indeed photographs indicate that the boundary between the dye and the clear fluid is sharp, which implies that penetration by diffusion is relatively small. However, the photographs also show that the apparent dye area grows with time. The phenomenon is due mostly to the photographic technique. That is, the observed dye area consists of the actual dye area (which is constant if diffusion is negligible) plus an apparent area due to width and glowing effects. Since the striations have depth, and the camera is not infinitely far away from the observation region, the camera is able to 'see' part of the lateral area of the stretched and folded striations (see figure 8). Also, when striations get very close together, the camera is unable to distinguish them. In our particular configuration, we estimate that when two striations are closer than 10 μm, they are indistinguishable; eventually when the mixing is widespread the entire cavity appears to be dye-filled. Also, glowing effects, analogous to a light bulb that seems to appear bigger when it is illuminated, contribute to the creation of apparent area. This effect depends on the exposure time; longer exposure time causes striations to appear thicker. One possible and partial solution to both width and glowing effects

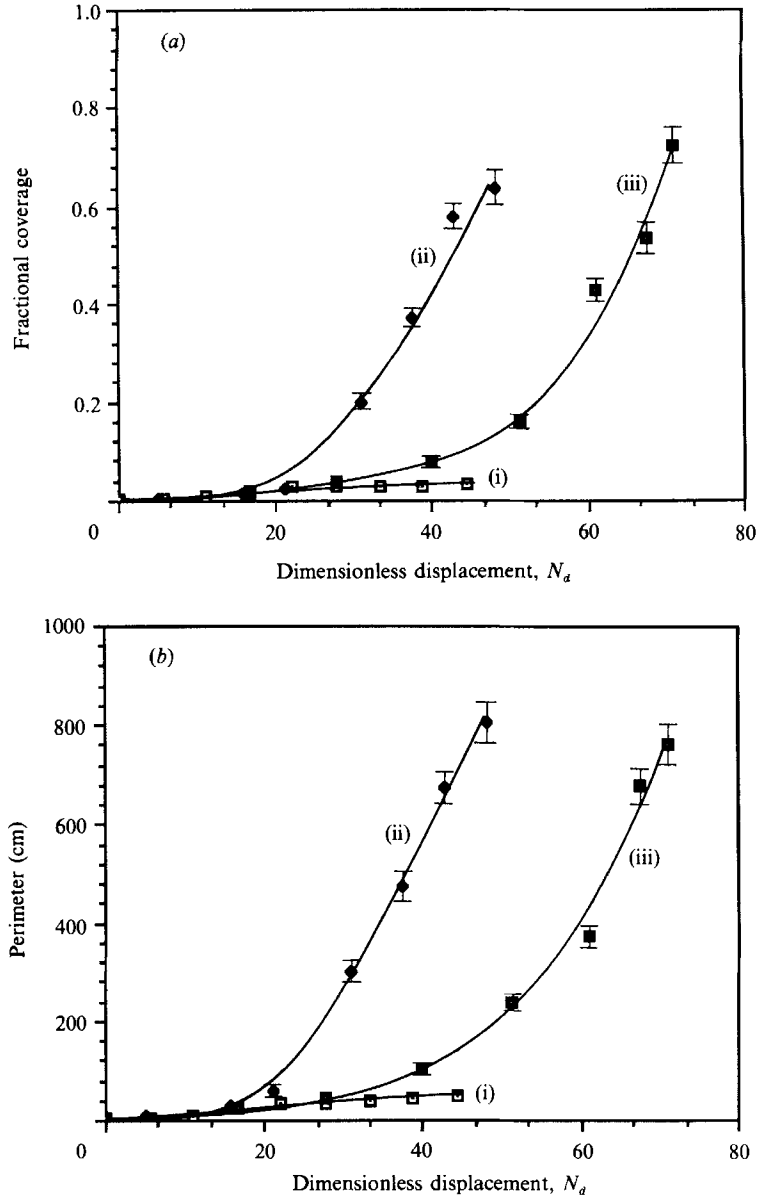

FIGURE 9. (*a*) Fractional coverage and (*b*) perimeter growth of dye apparent area as a function of dimensionless wall displacement for three classes of flows: (i) steady flow with one wall moving, (ii) discontinuous corotational flow ($D = 10.65$), and (iii) sinusoidal corotational flow ($D = 6.49$). Both time-periodic flows produce exponential growth ($\exp(\beta N_d)$) in fractional coverage, A, and perimeter, P, with approximately the same exponent β($\beta = 0.022 \pm 0.001$ s^{-1} for the discontinuous flow and $\beta = 0.019 \pm 0.001$ s^{-1} for the sinusoidal flow). Both A and P grow linearly with dimensionless wall displacement in the steady flow.

is to reduce the visible depth of the dye. This can be achieved by slicing the dye across the two-dimensional plane with a UV laser; preliminary experiments have shown this to be an effective technique. However, the area growth can be used to our advantage. An area count yields the perimeter between the fluids. In fact, a rough calculation suggests that the perimeter is directly proportional to the apparent area

of the dye, and quantitative image analysis measurements suggest that this is indeed true (see figure 9). Obviously, the observed area is bounded by the size of the cavity, while the perimeter is not, and therefore the proportionality between perimeter and area holds as long as the cavity is not completely dye-filled. A second important advantage is that it is much easier to measure area (count pixels) rather than to measure the perimeter of the dye.

The image analysis system used in the experiments is an Analytical Imaging Concepts model M/T-100, including morphometric measurement software which is capable of measuring the area coverage and perimeter of the dye. Both programs are independent; the measurement of area is based on pixel counting; the measurement of the perimeter is based on counting perimeter sites after image enhancement by thresholding followed by differentiation. It is important to note that the perimeter measured will be always somewhat lower than the actual perimeter since the picture loses resolution when transferred from the TV camera to the VCR and finally to the computer. In particular, striations of the same order of magnitude as the pixel size are lost. The measurements are somewhat dependent upon the threshold value, which is set based upon the histogram of the pixels values. However, since the contrast between the dye (white) and the bulk fluid (black) is relatively sharp, the histograms usually show two peaks, and the dependence upon threshold is, therefore, rather small. Figure 9 shows typical area and perimeter growth as a function of mixing time for three systems: (i) one wall moving, (ii) discontinuous flow with $D = 10.65$, and (iii) sinusoidal flow with $D = 6.49$. Figure 9(*a*) shows that the two unsteady flows have exponential area stretching of the form $A = A_0 \exp(\beta t)$, where $\beta = 0.022\ \mathrm{s}^{-1} \pm 0.001\ \mathrm{s}^{-1}$ for the discontinuous corotational flow and $\beta = 0.019\ \mathrm{s}^{-1} \pm 0.001\ \mathrm{s}^{-1}$ for the sinusoidal corotational flow; the error bar is computed based on a variation of the threshold value by ± 20 out of 256 grey units. However, the steady-flow stretching is linear, and at the completion of the experiment, it is two orders of magnitude lower than the periodic flows. The perimeter growth is shown in figure 9(*b*) and follows $P = P_0 \exp(\kappa t)$ for the periodic flows, and is linear for the steady flow. Significantly, $\beta = \kappa$, within experimental error, in both time-periodic flows for area coverages of less than 50%. More importantly, the exponent β can be viewed as an average Liapunov exponent and, since it is positive, it indicates that the time-periodic flows are, in general chaotic. It should be noted that the stretching rate is only indicative of how fast the dye is being stretched and it is, therefore, a poor indication of the dispersion of the dye throughout the cavity.†

4.2. *Mixing behaviour as a function of D*

In order to further understand the mechanisms of chaotic mixing we undertook a study focusing on the changes of the mixing behaviour as a function of the parameter D.

† It should be pointed out that, owing to the existence of islands of unmixed material, it is rather inappropriate to speak of average striation thickness of the flow especially when the island lengthscale is several orders of magnitude larger than the average striation thickness in the chaotic regions. There is clearly a need to develop more general ways of quantifying the state of the mixture. One possible way is to measure the fractal dimension of the stretched and folded structure. Measurements conducted by Professor Sreenivasan of Yale University, on some of our experimental results, indicate that the chaotic structures (for example, figure 7*d*) have a dimension of approximately 1.9, which is very close to a space-filling curve. As expected, it is not possible to estimate the fractal dimension of the structures produced in steady flows such as figure 7(*a–c*); the structures are not fractals since there is no repetitive mechanism that producing stretching and folding.

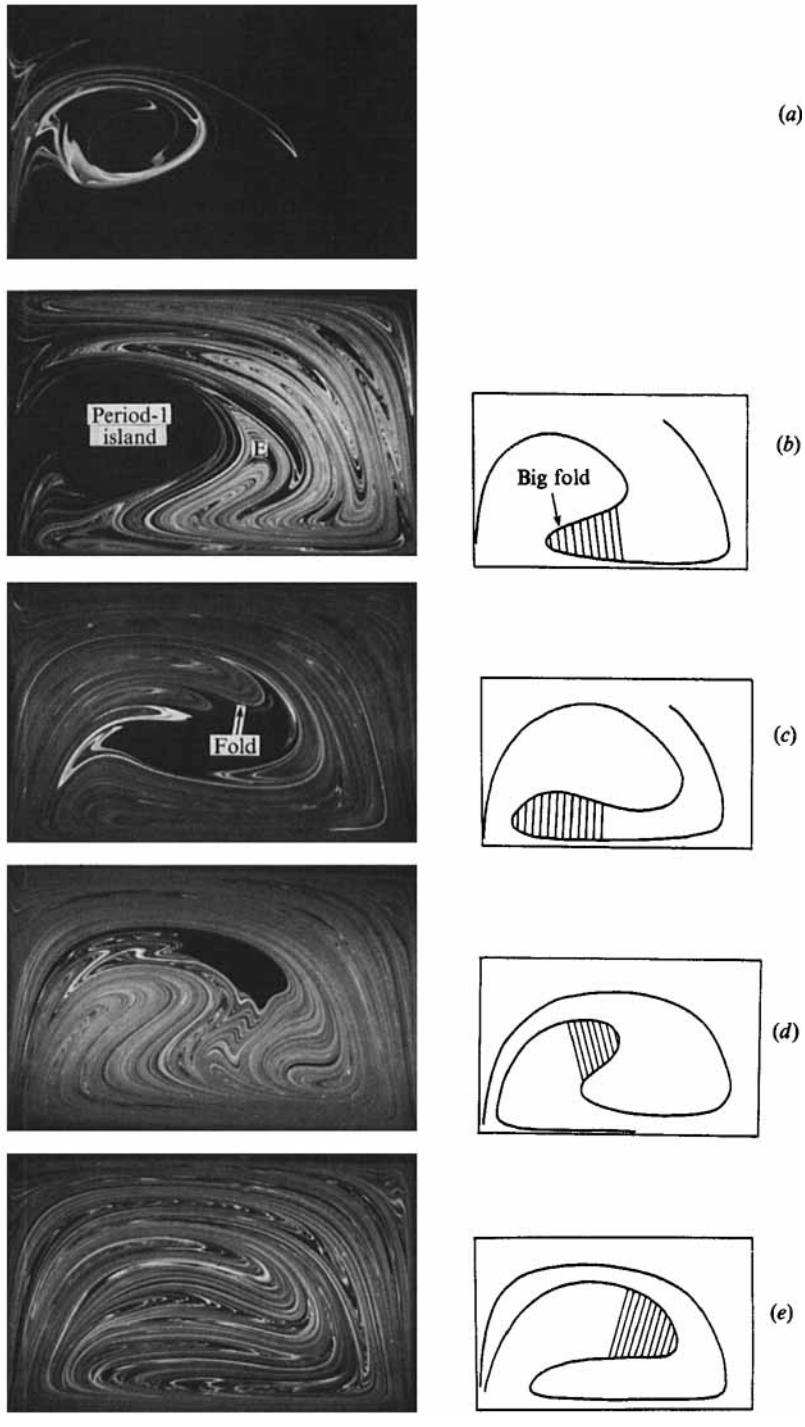

FIGURE 10. For caption see facing page.

We also pay particular attention to growth, collapse, and bifurcation of large islands. Most of the experiments start with an initial condition involving a blob of approximately 7 mm in diameter located 1.27 cm from the left static wall along the x-axis, as shown in figure 3(*a*)(i), unless otherwise indicated. In some cases, however, two blobs are needed to trace out the bulk of the structures (see figure 3*b*). The experiments presented here are carried out long enough to clearly reveal the mixing structures, but not so long as to lose the resolution owing to diffusion. The typical duration of the experiments is about five minutes, the number of periods is in the order of 10, and the corresponding number of wall displacements N_d is about 90. The discussion begins with the discontinuous flow and is then followed by the sinusoidal flow. We complete the discussion by comparing the mixing produced by both flows with equal wall displacement per period and symmetry.

4.2.1. *Discontinuous corotational flow*

The results shown in figure 10(*a–e*) correspond to the discontinuous corotational flow. Note that the initial condition for (*b*) is located 1.27 cm away from the right static wall along the x-axis (figure 3*a*(ii)), while the others correspond to figure 3(*a*)(i). The main experimental result is the annihilation (or collapse) of a large period-1 island, as D increases from 6.24 to 12.85. Some of the results can be rationalized by means of a geometrical analysis. Close inspection reveals a 'big fold' which appears to grow with increasing D, shown schematically in figure 10(*b–e*). The growth is due to the fact that a larger D implies larger wall displacement per period. This particular 'big fold' is of interest because as it grows, it wraps within itself, causing the island to shrink until it collapses completely.

The details of the process appear to be rather complicated. When D increases from 6.24 to 8.44, the boundary of the island changes from smooth to irregular (note the multiple folds along the island boundary in figure 10*c*). The appearance of multiple folds indicates instability; we observed repeatedly that *whenever an island boundary exhibits multiple folds*, the island collapses or bifurcates upon a further increase in D. At $D = 10.65$ (figure 10*d*), the island shrinks substantially, and at $D = 12.85$ (figure 10*e*), the island disappears (further details are given in §4.3.1).

Islands obstruct transport. An example of what happens when a blob of dye is located close to the island boundary is shown in figure 10(*a*). This system has the same value of D as the system corresponding to figure 10(*b*), except that in 10(*b*) the initial blob is located outside the island. Figure 10(*a*) shows that part of the blob is stretched and dispersed along the island boundary. If the experiment is continued,

---

FIGURE 10. Illustration of chaotic mixing produced by a discontinuous corotational flow ($Re = 1.2$). The top wall moves from left to right for half a period, $\frac{1}{2}T$ and stops, the bottom wall moves from right to left for half a period, $\frac{1}{2}T$, and then stops, and so on (cf. figure 4*a*). There is a 5 s pause between half-periods to reduce inertial effects. The governing parameter is the dimensionless wall displacement D: (*a–e*) correspond to $D = 6.24$, 6.24, 8.44, 10.65, and 12.85, with their corresponding $N_d = 62.8$, 62.8, 73.4, 106.3, 64.3, respectively. The initial condition for (*b*) corresponds to figure 3(*a*)(ii), while (*a*, *c–e*) correspond to figure 3(*a*)(i): (*a*) is an example of mixing of a blob initially located close to the boundary but in the interior of an island; note that the flow conditions are the same as (*b*) except that the initial blob in case (*b*) is located outside the island. In this case, we observe an island of period-1 collapsing and disappearing as D increases from 6.24 to 12.85. Note the lump structure surrounding the island in (*c*); such a structure is indicative of the instability of the island. The sketches on the right-hand side of (*b–e*) depict a 'big fold' that grows with increasing T and squeezes out the central island.

the dye located outside the boundary is stretched and dispersed all over the chaotic region, such as shown in figure 10(*b*). A comparison between figures 10(*a*) and 10(*b*) reveals the size and shape of the island. However, if the blob is located close to the centre of the island it would be trapped indefinitely and it would not stretch significantly within the timescale of the experiment (see time-sequence in Ottino 1989*b*).

The E shown in figure 10(*b*) denotes another kind of region which is not dye-filled. However, can we regard these empty regions as islands? According to our definition, an island is a region such that (i) it is not dye-filled, (ii) the flow within it is mostly rotational, and most importantly, (iii) it stays as a hole without dye for an indefinite amount of time. Within the resolution of our experiments and based upon the cases studied, the answer seems to be no. The black regions located within the folds usually disappear upon further mixing. However, we recognize that the experimental technique might be too coarse to identify small islands located within the space left between folded striations ('incomplete folds', see Ottino *et al.* 1988).

4.2.2. *Sinusoidal corotational flow*

For the sinusoidal corotational flow, we investigate two cases: $\alpha = \frac{1}{2}\pi$, $\frac{1}{4}\pi$ (see (2.1) and (2.2)). The first case, $\alpha = \frac{1}{2}\pi$, is analysed and compared briefly with the discontinuous flow. The second case, $\alpha = \frac{1}{4}\pi$, is analysed and compared with the first case to determine how the changes in α affect the overall mixing.

The instantaneous streamlines of the flow with $\alpha = \frac{1}{2}\pi$ form closed orbits with an elliptic point moving from $y \approx \frac{1}{6}H$ to $-\frac{1}{6}H$ along $x = 0$ in a time-periodic fashion; the streamlines evolve smoothly from top wall moving (figure 5*a*), to two walls moving in the opposite directions (figure 5*c*), to bottom wall moving (i.e. such as figure 5*a* but rotated by 180°), and so on. Note that the evolution is smooth and not sudden as in the discontinuous case. Results corresponding to $\alpha = \frac{1}{2}\pi$ are shown in figure 11 (for figure 11*a–d* see Plate 1). Figure 11(*a–c*) corresponds to experiments conducted with two blobs (green and yellow). The initial locations of the blobs are as shown in figure 3(*b*). On the other hand, figure 11(*d–g*) corresponds to experiments conducted with only one blob located near the left static wall (figure 3*a*(i)). Figure 11(*a*) shows the coexistence of two mutually exclusive chaotic regions. These regions do not mix even after a long time, yet it can be observed that both blobs are being stretched and folded significantly. Furthermore, the red region exhibits three period-3 islands (which correspond to the 'eyes' and 'mouth' of a 'face') surrounding a period-1 island (the 'nose'). Notice also that the arrangement of the islands is symmetric with respect to the vertical axis (this is particularly clear in figure 11*a–c*). As D increases from 3.90 to 4.16 (figure 11*b*), the boundary disappears, and the green and the yellow dyes begin to mix, although it can still be observed that the green dye has not penetrated inside the yellow region; the 'face' still can be recognized (i.e. the islands surrounding the periodic points are still visible). The mixing only occurs around the red region, where the yellow folds intermingle with the green folds. At a larger value of D (= 4.42, figure 11*c*), the green and the yellow dyes completely mix. However, at this operating condition, the overall mixing is bad, since several large islands appear; at this point, remnants of the old 'face' are still evident; however, several other structures, rather similar to those in (*a*), appear (this is the experiment displaying the clearest symmetry we have seen in all our experiments). When D is increased further to 5.19 (figure 11*d*), all the large islands collapse. But, beyond $D = 5.19$ (figure 11*e*, *g*), a large period-1 island appears and grows with increasing D. The optimum mixing seems to be at $D = 5.19$. The overall behaviour of this system is therefore different to that of the discontinuous protocol (figure 10).

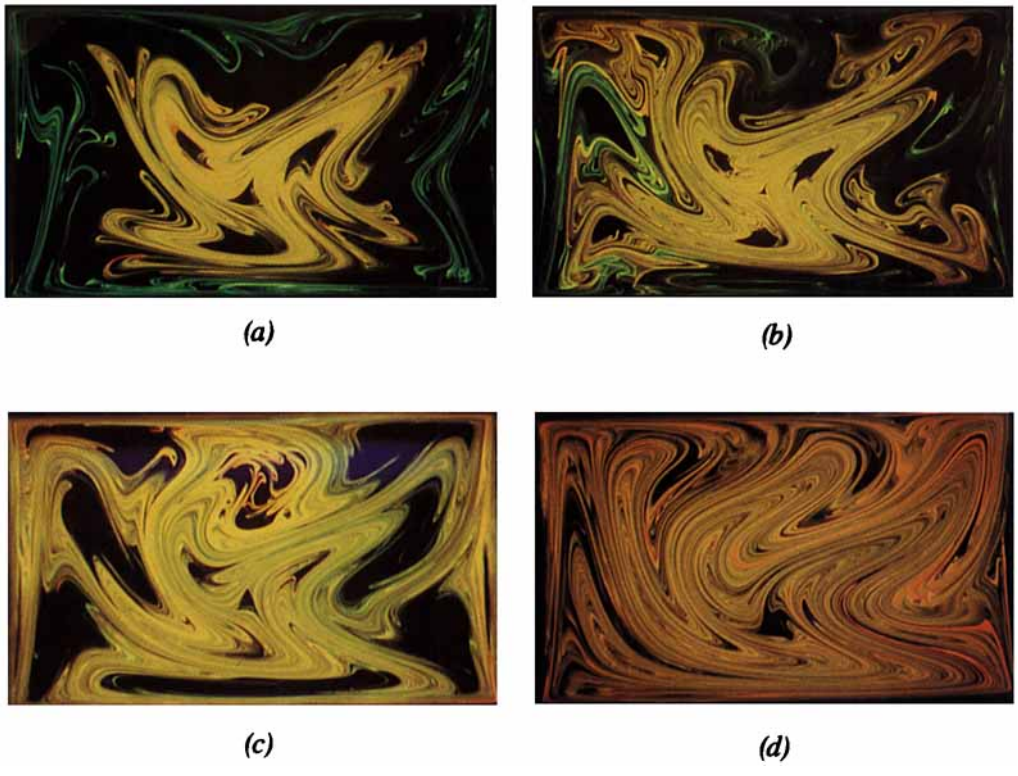

FIGURE 11(*a-d*). For caption, see facing page.

(*e*)

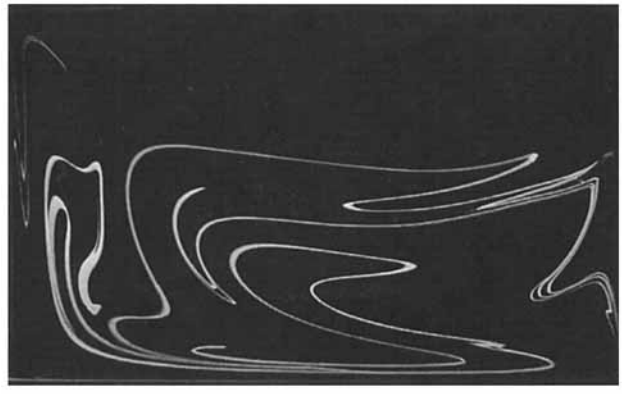

(*f*)

(*g*)

FIGURE 11. Illustration of chaotic mixing produced by the sinusoidal flow which corresponds to (2.1) and (2.2) with $\alpha = \frac{1}{2}\pi$ ($Re = 1.7$ and $0.10 < Sr < 0.20$). The pictures are taken at the instant when the top wall and bottom wall are moving at maximum and minimum (zero) speed, respectively. The governing parameter D is (*a*) 3.90, (*b*) 4.16, (*c*) 4.42, (*d*) 5.19, (*e*) 6.49, (*f*) 7.79 and (*g*) 7.79, and their corresponding N_d is (*a*) 156.0, (*b*) 166.4, (*c*) 176.8, (*d*) 72.7, (*e*) 91.9, (*f*) 39.0 and (*g*) 109.1. (*a–c*) Experiments conducted with two blobs (green and yellow), the initial locations of the blobs are as shown in figure 3(*b*); (*d–g*) experiments conducted with one blob located near the left static wall (figure 3*a*(i)). At small D values (*a* and *b*), the system exhibits two chaotic regions (green and red) that do not interact or mix. At $D = 4.42$ (*c*), the system displays many large islands. At $D = 5.19$ (*d*), all the large islands collapsed, and the system becomes well mixed (near global chaos). But, beyond $D = 5.19$ (*e*, *g*), a large period-1 island appears and grows with increasing D. (*f*) illustrates the rapid delineation of a large-scale chaotic structure; (*f*) and (*g*) have the same value of D. (*f*) corresponds to 5 periods and (*g*) to 14 periods. Note that the outline of the macroscopic structures of (*g*) is already visible in (*f*).

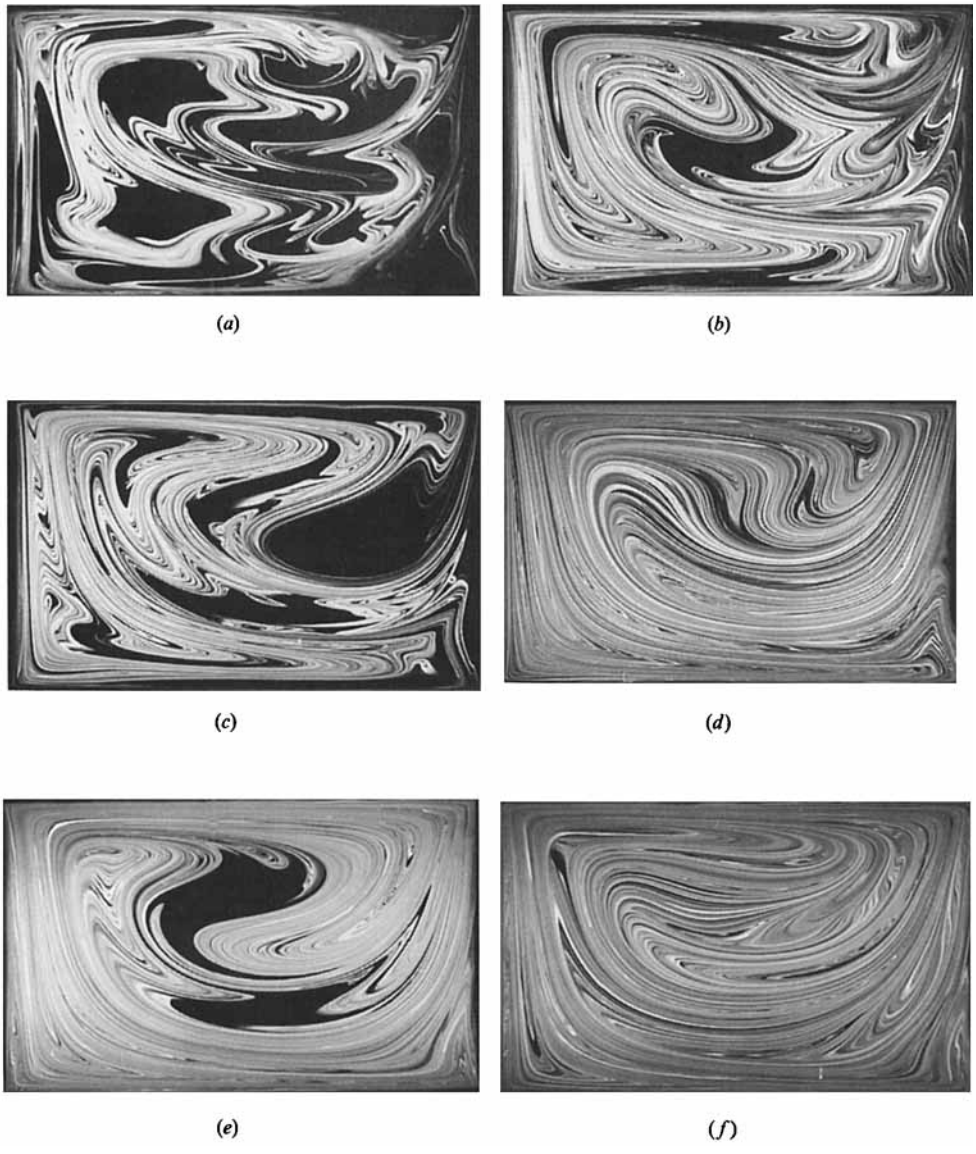

FIGURE 12. Chaotic mixing produced by the sinusoidal flow ((2.1) and (2.2)) with the phase angle $\alpha = \frac{1}{4}\pi$. The governing parameter D is (*a*) 5.19, (*b*) 6.49, (*c*) 7.79, (*d*) 9.09, (*e*) 10.39, and (*f*) 11.69, with a corresponding displacement N_d of (*a*) 311.6, (*b*) 260.0, (*c*) 187.0, (*d*) 181.7, (*e*) 145.4, and (*f*) 187.0, respectively. The initial condition corresponds to figure 3(*a*)(i). At $D = 5.19$, (*a*), the system exhibits many islands which hinder the mixing significantly. This is why the experiments are conducted for a very long time (indicated by the relatively large values of N_d). The sequence of events from $D = 5.19$ to 11.69 is rather complex; islands appear and disappear, and at two different values of D (9.09 and 11.69) there are no observable islands left.

We also observed that the macroscopic structures are delineated rapidly; finer details can be observed after a larger number of periods, while the macroscopic structures remain essentially unchanged. This behaviour is illustrated in figure 11 (*f*, *g*). Notice that the outline of the macroscopic structures at 14 periods (figure 11*g*) are already visible after just 5 periods (figure 11*f*). The main difference is that there are

simply more folds after 14 periods than after 5. However, the large period-1 island remains virtually unchanged.

Consider now a similar series of experiments using the sinusoidal corotational flow, but with $\alpha = \frac{1}{4}\pi$. The results are shown in figure 12. In general, this system behaves very differently from the previous two systems. Initially, at $D = 5.19$ (figure 12*a*), the system exhibits many regions of islands which inhibit effective mixing. In fact, because of the presence of islands and slow mixing, the experiment needs to be run for an unusually long time (indicated by the value of N_d) to successfully trace the chaotic regions. At $D = 6.49$, figure 12(*b*), there are two thin islands stretched out along the moving walls and an island located at the centre of the cavity. Then at $D = 7.79$ (figure 12*c*), the islands are clearly defined, with a period-1 island close to the right static wall. Around the period-1 island, there are two period-2 islands. Subsequently, at $D = 9.09$ (figure 12*d*), all the islands disappear and the cavity is almost completely dye-filled; the picture is similar to that of figure 10(*e*) when rotated by 180°. At $D = 10.39$ (figure 12*e*), two large period-2 islands appear; note the irregularities of the island boundary. Finally, at $D = 11.69$ (figure 12*f*), the two islands collapse and the system is completely dye-filled again; again the picture is very similar to that of figure 10(*e*) when rotated by 180°. Obviously, the system must have gone through a series of bifurcations as D varies from 5.19 to 11.69. Note also that the 'maximum' amount of chaos (i.e. when the cavity is completely dye-filled from a qualitative viewpoint) occurs at more than one value of D (e.g. see results corresponding to $D = 9.09$ and 11.69, figures 12*d* and 12*f*, respectively).

The islands and the macroscopic structures observed in these experiments are quite robust. Their location, size, and shape can be reproduced with little difficulty. However, upon close observation, it is possible to detect minor differences in the local structures, such as more or fewer folds within folds or the small folds might be folded in different ways. For example, in spite of some minor local differences, two different experiments such as figures 10(*d*) and 14(*e*) (produced under the same operating conditions) appear to be identical; the 'fitting' between figures 10(*a*) and 10(*b*) is even more remarkable. Undoubtedly, given the chaotic nature of the flows, the differences are highly dependent on the initial size and the location of the blob, factors which are impossible to reproduce exactly experimentally.

4.2.3. *Comparison between discontinuous flow and sinusoidal flow*

It appears that the structures produced by the sinusoidal corotational flow ($\alpha = \frac{1}{2}\pi$) are quite different from the structures produced by the discontinuous corotational flow. The overall behaviour seems to be directly opposite; the sinusoidal flow has an island which grows in size with D whereas the discontinuous flow has an island which decreases in size with D. This seemingly opposite behaviour might be due to an incorrect comparison and it is important to investigate other possibilities.

In fact, the two flows reveal enlightening similarities when they are compared on an appropriate basis. A suitable comparison can be made in terms of the following two criteria: (i) the two flows have approximately the same value of D, and (ii) the two flows have *identical symmetry* at the instant the picture is taken. In a broad sense, we search for similarities in the macroscopic structures of the flows (islands and large-scale folds). This idea can be made precise by means of symmetry arguments (see the Appendix). A symmetry is a vector operator which places geometrical restrictions on the motion of a fluid particle (Greene *et al.* 1981; Franjione, Leong & Ottino 1989). For example, the geometry of the streamlines corresponding to the steady cavity flows (figure 5) is symmetric with respect to

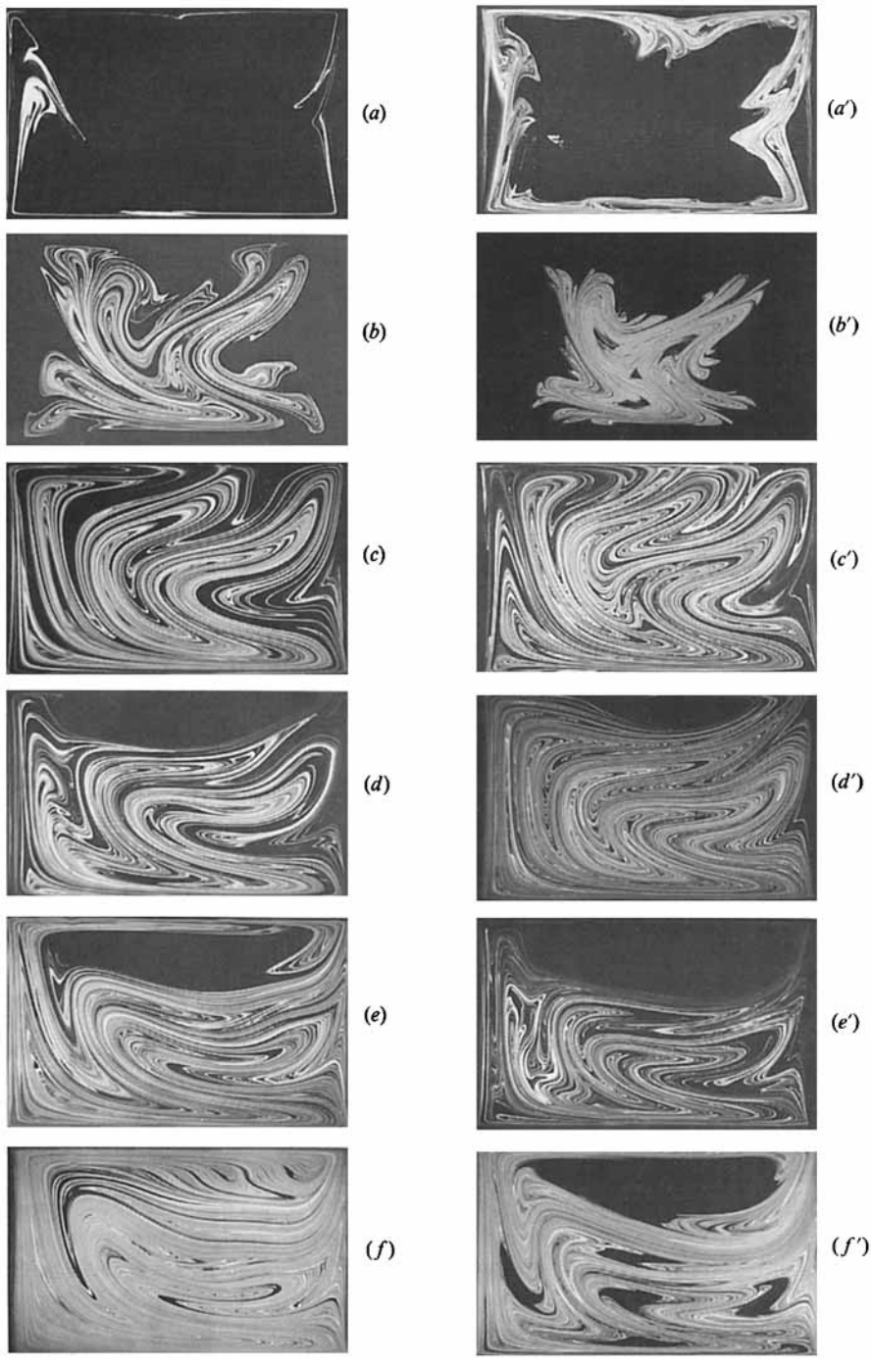

FIGURE 13. For caption see facing page.

reflections about the y-axis. In the two time-periodic flows, the y-axis symmetry can be observed if the following conditions are satisfied,

$$v_{\text{top}}(t-\tfrac{1}{2}T) = v_{\text{top}}(\tfrac{1}{2}T-t), \quad v_{\text{bot}}(t-\tfrac{1}{2}T) = v_{\text{bot}}(\tfrac{1}{2}T-t).$$

These conditions impose a restriction on the v_{top} and v_{bot} to be even about the half-period $\frac{1}{2}T$ (see Appendix for derivation). In this particular situation, we can compare the sinusoidal flow and the discontinuous flow when we define the period of the discontinuous flow as follows: the top wall moves for $\frac{1}{4}T$ and the bottom wall moves for $\frac{1}{2}T$, and finally the top wall moves for $\frac{1}{4}T$; note that the starting and ending conditions are different from the previous experiments. In this case, both flows are even about $\frac{1}{2}T$, thus possessing the y-axis symmetry. In short, the reason for condition (ii) is to determine when is the right time to stop and take a picture, such that the macroscopic structures are comparable. It is important to note that in these experiments criterion (ii) plays a more significant role than criterion (i).

The results are shown in figure 13 (the figures with a prime denote the sinusoidal flow, those without a prime the discontinuous flow). For small values of D, both systems appear similar; however, at large values of D, the similarities diminish. Figures 13 (a) and 13 (a') and 13 (b) and 13 (b') are similar, both have invariant surfaces close to the boundary of the cavity and similar internal structures, except that the size is different. Figures 13 (c) and 13 (c') also show similar structures; however, the similarities diminish quickly from figures 13 (d) and 13 (d') and beyond.

Note that if condition (ii) is not imposed, the two systems are not readily comparable. A clear example is seen by comparing figures 10 (b) and 13 (d) where both systems have approximately the same wall displacement per period (D) but different symmetry. The main reason for the dissimilarity is that the macroscopic structures and the islands move about in the cavity (see figure 15). Thus, by stopping at the precise moment, similarities between the two systems can be observed. For example, if we allow the system corresponding to figure 10 (b) to continue for another quarter of a period (with the top wall moving) the resultant structure and the location of the island would look very similar to that of figure 13 (d). Here we have illustrated that incorrect comparisons can be very misleading and, therefore, caution must be taken in interpreting results from one system and extrapolating them to another.

FIGURE 13. Comparison of chaotic mixing between the discontinuous corotational flow and the sinusoidal corotational flow ($\alpha = \frac{1}{2}\pi$) at equal wall displacement per period and the same symmetry at the instant that the picture is taken. The initial condition is a blob of fluorescent dye located near the left static wall (see figure 3a). The sinusoidal flow corresponds to (2.1) and (2.2) with periods D of (a') 3.90, (b') 3.90, (c') 5.19, (d') 6.49, (e') 7.79, and (f') 9.09, with corresponding N_d of (a') 156.0, (b') 156.0, (c') 72.7, (d') 90.9, (e') 140.3, and (f') 109.1, respectively. (a') and (b') show that there are two distinct regions separated by an invariant surface; the initial condition for (b') is located at the centre of the cavity. The period of the discontinuous corotational flow is defined as the top wall moving for quarter of a period, $\frac{1}{4}T$, and the bottom wall moving for half a period $\frac{1}{2}T$, and then the top wall moving for another quarter of a period $\frac{1}{4}T$. The parameter D has the following values: (a) 3.96, (b) 3.96, (c) 5.36, (d) 6.70, (e) 8.07, and (f) 9.39, and their corresponding N_d are (a) 59.4, (b) 79.2, (c) 53.6, (d) 74.4, (e) 56.5, and (f) 75.2, respectively. The initial condition for (b) is located at the centre of the cavity. In general, the results show similarities of macroscopic structures when D is small, e.g. (a'–a) and (b'–b). However, the similarities disappear quickly for large values of D. The general behaviour, for both systems and that over the range of D studied, is similar; a period-1 island grows in size, then goes through various bifurcations, and finally collapses into many small high-period islands.

4.3. *Analysis of specific cases*

In this Section, we single out a typical operating condition to illustrate the bifurcation, birth, and collapse of islands. Another condition is singled out to demonstrate the application of a technique for finding periodic points and their orbits.

4.3.1. *Bifurcation, birth, and collapse of islands*

Generally, when an island collapses, the chaotic region tends to become larger. However, the process is rarely so simple. In some situations, an island goes through a bifurcation and gives birth to two or more smaller islands. For example, the central elliptic point of an island might become hyperbolic, and subsequently can give birth to two elliptic points of the same or higher order. Clearly, it is important to conduct experiments that might help to unravel the mechanisms leading to island collapse or bifurcation.

As a typical case we selected the discontinuous flow, since it has a relatively large island to begin with. Initially, we conjecture that the period-1 island, at $D = 8.44$ (figure 10*c*), goes through a bifurcation, and at $D = 10.65$ (figure 10*d*), the bifurcation has already occurred. The conjecture is based upon observing the characteristics of the island boundary, such as the multiple folds around it at $D = 8.44$; as mentioned earlier, multiple folds along the island boundary are indicative of the instability of an island. Unfortunately, the actual process is substantially more complicated. Figure 14 shows the frames corresponding to intermediate displacements between $D = 8.81$ and $D = 12.30$. Here we observe that the period-1 island indeed goes through a bifurcation, at $D = 8.92$ (figure 14*b*), in which two smaller period-1 islands are born. The bifurcation point is identified when the dye manages to penetrate through the centre of the island. Furthermore, the elliptic point that corresponds to the period-1 island becomes a period-1 hyperbolic point after the bifurcation.

The bifurcation shown in this experiment is a period-doubling bifurcation. In this particular case the island bifurcates and gives rise to one hyperbolic and two elliptic points. The original island, located precisely at the centre of the cavity, is actually of period $\frac{1}{2}$; that is, the island comes back to the same location after just half a period (i.e. moving the top or bottom wall only). However, strictly speaking, there is no such thing as a period-$\frac{1}{2}$ point, since the most fundamental period is 1, and therefore the island is denoted as period-1. After the bifurcation, the two newborn islands are of period-1, but the hyperbolic point continues to be of period-$\frac{1}{2}$. The islands switch positions after half a period whereas the central hyperbolic point returns to the centre of the cavity after half a period. Note, however, that the period-doubling route does not have to occur in area-preserving systems and that other mechanisms are possible (see Khakhar, Rising & Ottino 1986).

A naïve analysis based on a few photographs (for example, figure 10) might suggest that the island decreases in size (without bifurcation) from $D = 6.24$ to 12.85. However, we have just seen that this is not true, and that the process is considerably more complicated. The island collapses and is born again with just a small change in the period D (≈ 0.11). Earlier, in §4.2, we pointed out that the period-1 island may have been destroyed by the 'big fold' that grew with increasing D. We also hinted at another possible reason, which is the instability of the island, based on the appearance of multiple folds. In general, the latter explanation is a more accurate description of this process. Thus, in order to capture all the essential details, it is

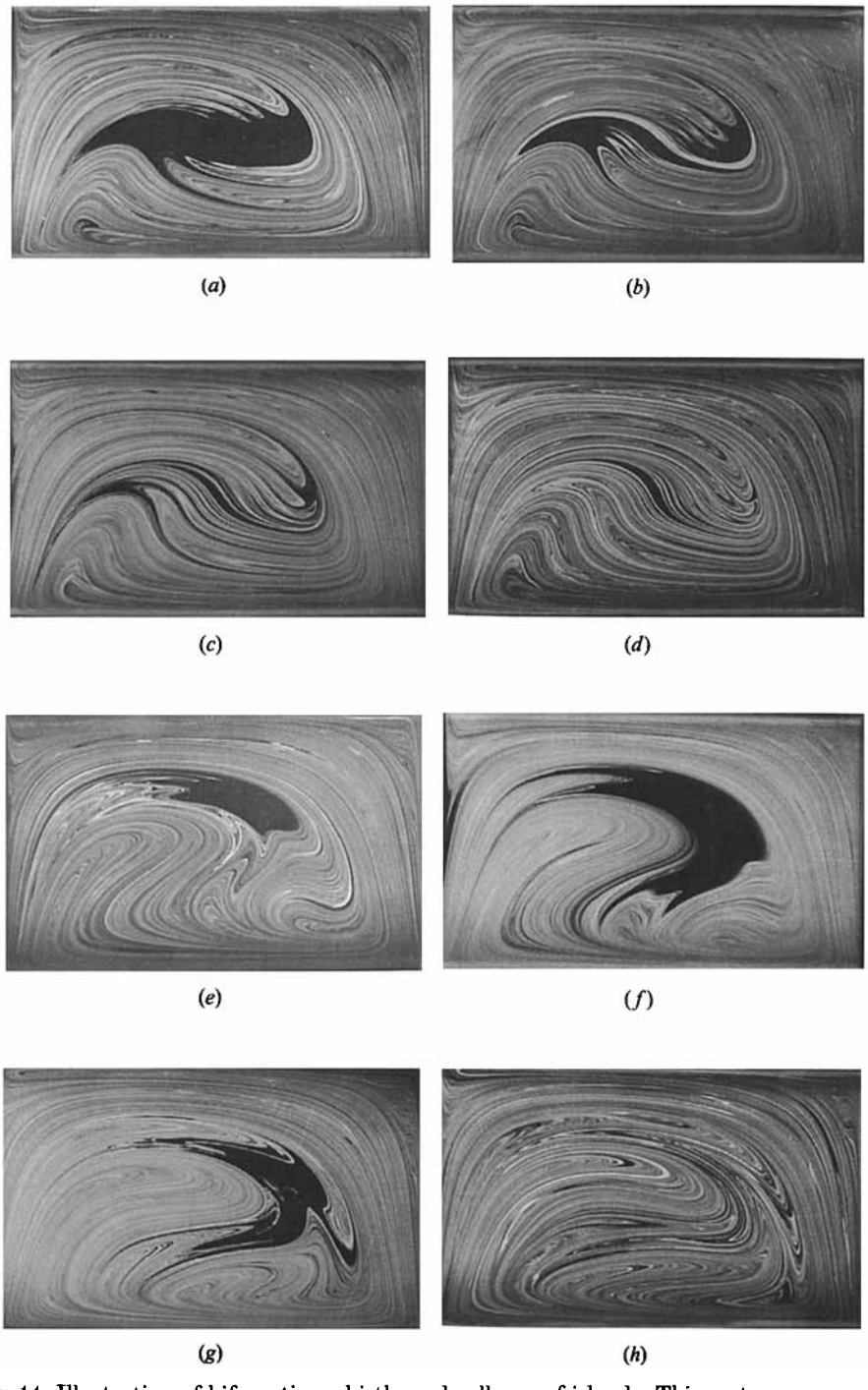

FIGURE 14. Illustration of bifurcations, birth, and collapse of islands. This system corresponds to a discontinuous corotational flow (cf. figure 10) in which the governing parameter D is (*a*) 8.81, (*b*) 8.92, (*c*) 9.07, (*d*) 9.25, (*e*) 10.65, (*f*) 10.94, (*g*) 11.86, (*h*) 12.3. The initial condition corresponds to figure 3(*a*)(i). The period-1 island, visible at $D = 8.81$, initially goes through a bifurcation at $D = 8.92$, giving birth to two period-1 islands, and itself becomes a period-1 hyperbolic point. As D increases further, the two new-born islands collapse and the period-1 hyperbolic point becomes elliptic again giving rise to another period-1 island. From then onwards, the island grows and finally collapses, shedding rings of small high-period islands at $D = 12.30$.

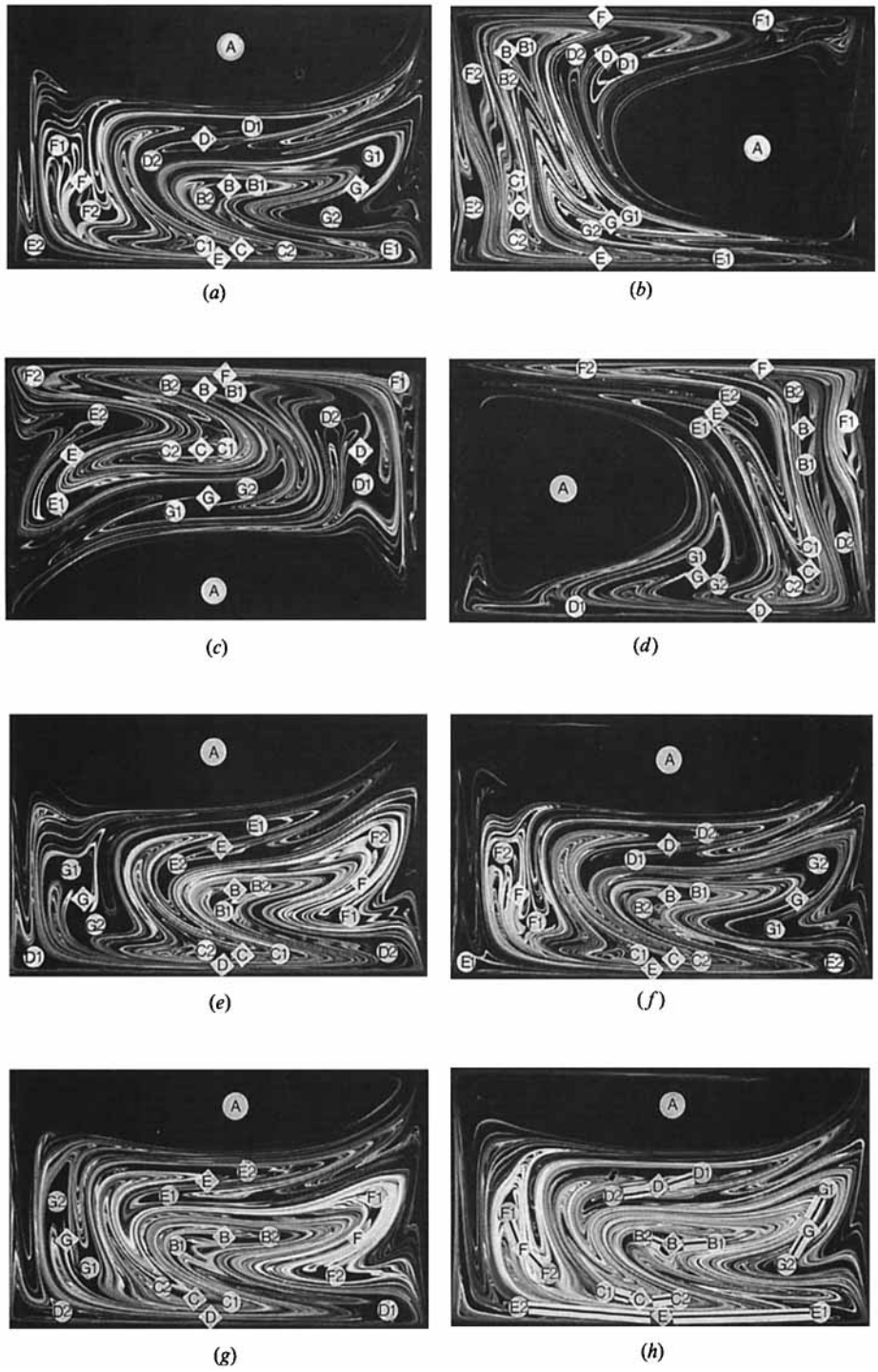

FIGURE 15. For caption see facing page.

necessary to conduct a thorough study by increasing D at very small intervals; however, this might not be possible in all cases and simple geometrical analyses might be the only choice.

As mentioned earlier, the experiments are highly reproducible. However, we found that whenever a system is close to or at the bifurcation point, the experiment is not easily reproduced and special precautions are necessary. For example, figure 14(*b*) shows the bifurcation of a period-1 island into two smaller islands. This experiment is not easily reproduced. Usually, when a replication is attempted, the result corresponds to the experiment either before or after the bifurcation. The problem is that, in order to reproduce the bifurcation experiment, the entire apparatus has to behave exactly the same way as before; the size and the initial location of the blob have to be identical. This is a nearly impossible demand from an experimental system. Otherwise, away from the bifurcation point, the experiments are robust and easily reproduced.

4.3.2. *Periodic points and coherent structures*

The coherence of structures helps in the identification and location of periodic points. Conversely, the motion of periodic points aids in visualizing the motion of the structure and identifying the regions of stretching and folding. The case chosen for the analysis corresponds to the sinusoidal corotational flow with $\alpha = \frac{1}{2}\pi$ and $D = 7.79$ (figure 11*g*).

We begin the analysis by locating periodic points. In practice, only low-order periodic points can be located. It is very difficult to observe higher-order ones, mainly because it takes a long time for them to appear. In addition, elliptic points are much easier to detect since they form islands. In order to locate the periodic points, we recorded the experiment on video tape and also made a poster consisting of 17 pictures taken at approximately $\frac{1}{4}$-period intervals, from period 10 to 14. Some of those pictures are shown in figure 15(*a–h*), which displays all the periodic points that we have located. For this experiment, Kodak T-MAX 400 ASA film is used, and the film is pushed to 1600 ASA so that the shutter speed can be set at $\frac{1}{32}$ s with an aperture of 4.0; the faster shutter speed is desired since we are interested in capturing the structures while the experiment is in progress. In this particular experiment, we were able to locate periodic points up to period-4. Note, however, this does not imply that we have located all the period-4 points.

The entire system behaves as a planetary one. 'Planets' (hyperbolic points) have 'moons' (elliptic points) with twice the period (figure 15*h*). There are altogether six such systems. In particular, there are four systems consisting of period-2 hyperbolic points surrounded by two period-4 elliptic points, and there are two systems

---

FIGURE 15. Visualization of the movement of periodic points and islands by means of instantaneous snapshots of the system corresponding to figure 11(*g*) taken at $\frac{1}{4}$-period intervals, from period 10 to period 14 (*a–h*). The symbols represent: A = period-1 island; B and C = period-1 hyperbolic periodic point; D, E, F and G = period-2 hyperbolic periodic point; B1, B2, C1 and C2 = period-2 elliptic periodic point; D1, D2, E1, E2, F1, F2, G1 and G2 = period-4 elliptic periodic point; the diamonds represent hyperbolic periodic points and the circles represent elliptic periodic points. In (*h*) the black lines connect two elliptic periodic points to a central hyperbolic periodic point, and all three points move as a unit (see Ottino *et al.* 1988). The period-2 hyperbolic periodic points, F and G, interchange their positions after one period; hyperbolic periodic points D and E also interchange their positions after one period.

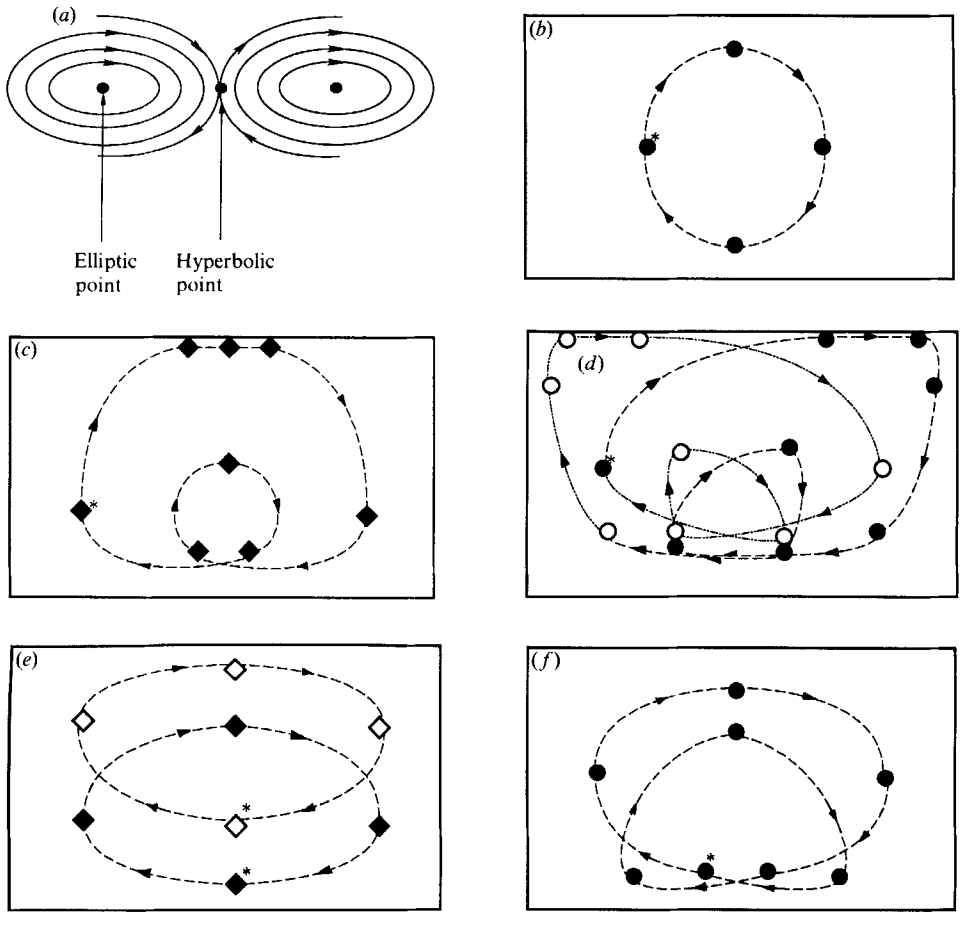

FIGURE 16. (*a*) The schematic of the flow in the neighbourhood of two elliptic periodic points and a hyperbolic periodic point. (*b–f*) The schematic of the orbits (particle paths) traversed by periodic points found in the system corresponding to figure 15: (*b*) shows the orbit traversed by a period-1 elliptic point, (*c*) by a period-2 hyperbolic point, (*d*) by a period-4 elliptic point, (*e*) two period-1 hyperbolic points, and (*f*) a period-2 elliptic point. The symbols, circles and diamonds, represent elliptic points and hyperbolic points respectively, and the spacing between symbols corresponds to $\frac{1}{4}$ of a period. The asterisk indicates the starting location and the arrow shows the direction of increasing time. In (*d*), the solid circles, which go with the broken line, represent the motion of the point throughout the first and second period; the open circles, which go with the solid line, the motion in periods 3 and 4.

consisting of period-1 hyperbolic points surrounded by two period-2 elliptic points. Figure 16(*a*) shows a schematic view of the arrangement of the two elliptic points belonging to the central hyperbolic point. As observed from figure 15, the four systems (with a period-2 central hyperbolic point) rotate around the other two systems (with a period-1 central hyperbolic point). There is a large island of period-1 which rotates in the clockwise fashion in the cavity. All the pictures are taken when the flow exhibits either x-symmetry (figure 15*b*, *d*) or y-symmetry (figure 15*a*, *c*, *e–h*). In this case the periodic points are located on the symmetry line or in pairs with respect to the symmetry line.

The analysis can be carried further to determine the orbits traversed by the periodic points and to infer the process of stretching and folding. The analysis reveals

five distinct particle paths or orbits: (i) period-1 island, (ii) period-1 hyperbolic points, (iii) period-2 hyperbolic points, (iv) period-2 elliptic points, and (v) period-4 elliptic points. The five types of orbit, shown in figure 16(*b–f*), are obtained from the 17 consecutive pictures by plotting the location of the point in question at $\frac{1}{4}$-period intervals. Each symbol (either circle or diamond) shown in the figure represents the location of the periodic point at successive $\frac{1}{4}$-period intervals. The circles represent elliptic points and the diamonds hyperbolic points; the asterisk indicates the starting location; the arrows indicate increasing time. Figure 16(*b*) shows the orbit traversed by the period-1 island, and it appears to be a simple circular motion; one can infer this orbit to be a period-1 orbit. Next, figure 16(*c*) shows the orbit traversed by a period-2 hyperbolic point, and this path seems to be much more interesting in that it forms two loops. Recall that there are two period-4 elliptic points belonging to each period-2 hyperbolic point and, referring to figure 15, one can see that the pair of elliptic points goes through a 360° rotation when the central hyperbolic point moves from the larger loop to the smaller loop. The orbit traversed by one of the period-4 elliptic points is shown in figure 16(*d*). This orbit is rather complex and it shows that the period-4 elliptic point visits a large portion of the flow domain; there are four loops for this particular period-4 orbit. Figure 16(*e*) shows the orbits of two period-1 hyperbolic points; recall that there is a pair of period-2 elliptic points belonging to each period-1 hyperbolic point (we purposely included two orbits to show that they overlap each other). Finally, figure 16(*f*) shows the orbit of a period-2 elliptic point. This orbit also has two loops, and is similar to the orbit traversed by the period-2 hyperbolic points. In a rough sense, the mixing process can be viewed as being produced by the motions of the periodic points – stirrers created by the flow itself. Good mixing in the chaotic region is due the interactions of the six stirrers; however, the overall mixing is poor because of the large unmixed region not visited by the stirrers and occupied by the large-scale island. In fact, rough sketches of mixing are possible; one can estimate how a line, with two ends initially located on two periodic points, would be stretched after 1, 2 or 3 periods. This exercise is also useful when one wants to know how individual parts of the flow communicate with each other.

5. Other related flows and conclusions

It is clear that the discontinuous and sinusoidal corotational flows described so far display a complex and rich behaviour. Even though these two cases are far from being completely understood, it is important to show the kinds of phenomena present in other related flows in order to gain an appreciation of the full scope of the problem at hand. However, we do not expect the exact features of our results to translate without modification to flows that are not topologically equivalent to the ones presented here or to flows that do not exhibit the same symmetries (topological equivalence means roughly that the instantaneous streamlines portraits of the flows can be deformed smoothly without change in topology to coincide with one another; the term symmetry is made precise in the Appendix). In this Section we consider briefly two possible flows that can be studied with our apparatus. The first flow is a variation of the sinusoidal flow of §4.2.2, but with both walls moving in the same direction (see (2.1) and (2.2); we take $U_{\text{top}} = -U$, $U_{\text{bot}} = U$, and $\alpha = \frac{1}{2}\pi$). In this case, the instantaneous streamlines evolve smoothly from one elliptic point (when the top wall is at maximum speed and the bottom wall at zero speed, see figure 5*a*) to two elliptic points (when top and bottom walls are moving at the same speed, see figure 5*b*), and then, back to one (when the top wall is at zero speed and the bottom is at

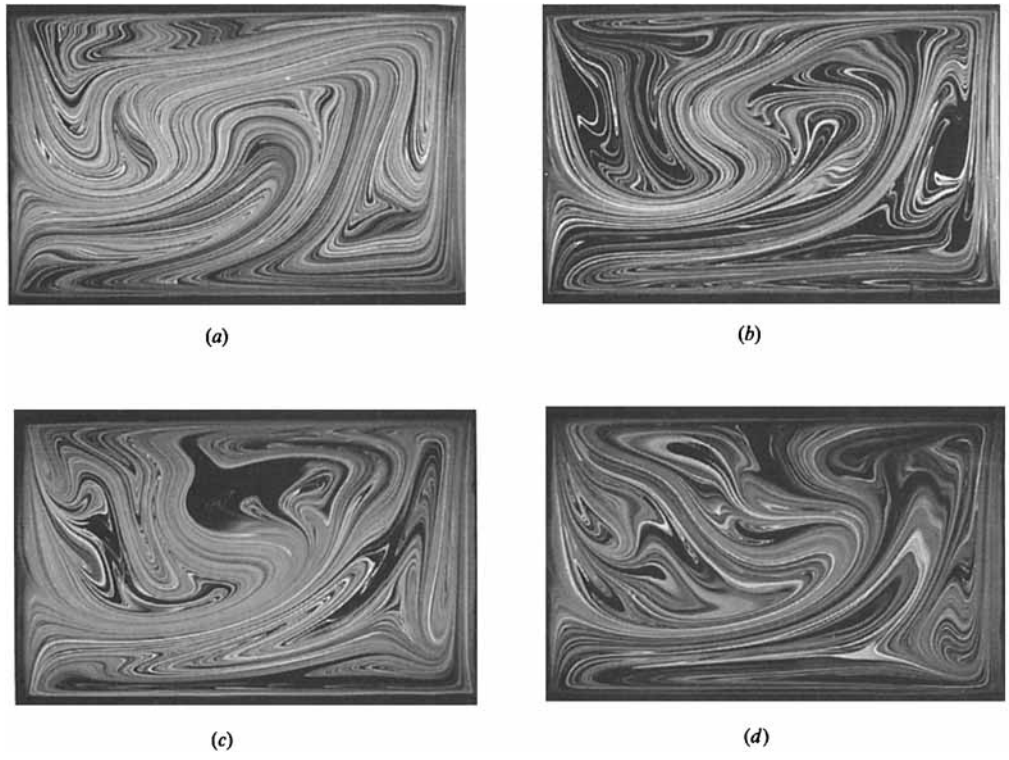

FIGURE 17. Mixing of a blob corresponding to the initial condition of figure 3(*a*)(i) under the sinusoidal flow of (2.1) and (2.2), but with both walls moving in the same direction. The governing parameter D has the values (*a*) 3.90, (*b*) 5.19, (*c*) 6.49, and (*d*) 7.79, while N_d is (*a*) 78.0, (*b*) 62.3, (*c*) 90.9, and (*d*) 93.5, respectively. Although the mixing in all four cases is quite good, the best seems to be at $D = 3.90$. In this case, there are no large islands forming or collapsing as in the previous cases of figures 10, 11, and 12. Observe that in (*a*), the folds are well 'packed' together and there are no observable islands. On the other hand, when the folds are not as well 'packed', such as in (*b–d*), small islands appear.

maximum speed, a picture like figure 5(*a*) but rotated by 180°); note that this flow has a reflectional symmetry (y-axis) and a rotational symmetry. The results indicate that the best mixing is at approximately $D = 3.90$ (figure 17*a*). Beyond $D = 3.90$, several small islands appear and eventually diminish in size. When observed closely, one can see a clearly defined macroscopic structure that changes in size and shape with D. During the changes, islands appear such as the ones seen at $D = 6.49$ (figure 17*c*). In general, this flow seems to mix better than the flows discussed in the previous Sections (figures 10 and 11). Note that the recirculation in this system is different than in the discontinuous or sinusoidal corotational flows. The fluid in the cavity can circulate in the clockwise or anticlockwise directions (owing to the transition from one elliptic point to two and vice versa); in the corotational flows the fluid always circulates in the same direction (clockwise in all our experiments).

Another flow which we are currently investigating is a corotating tall cavity with aspect ratio of 0.75 (figure 18*a*) which displays a hyperbolic point in the steady-state streamlines. When both walls are moving in opposite directions, the steady streamlines exhibit two elliptic points and a hyperbolic point at the centre of the cavity. The streamline portrait is reminiscent of that of the blinking vortex flow

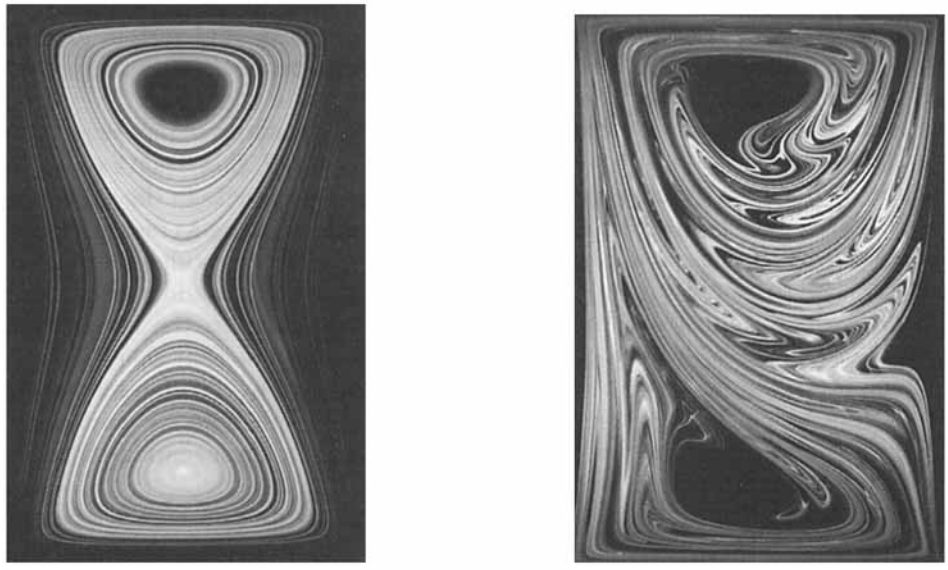

(*a*) (*b*)

FIGURE 18. (*a*) Steady-streamlines portrait of a cavity flow with an aspect ratio of 0.75 ($H = 6.2$, $W = 4.65$ cm). The streamlines are obtained by a line deformation experiment, where a line of dye is injected 5 mm below the free surface and along the y-axis of the cavity. The top and bottom walls are moving opposite in directions at the speed of 1.9 cm/s; the photographic techniques are described in §2.5. (*b*) Illustration of the chaotic mixing produced by perturbing the flow corresponding to (*a*) with a discontinuous wall motions; the top wall moves for 20 s and the bottom wall moves for 20 s ($D = 16.34$). There is a 5 s pause between the transition. The wall velocity is 1.9 cm/s. The experiment is carried out for a total of $N_d = 65.4$ (a total of 4 periods). Clearly, the mixing is chaotic.

(Aref 1984; Khakhar *et al.* 1986) except that the velocity increases gradually from the elliptic point and then decreases until reaching the static wall (and of course, v_θ is a function of θ as well). To illustrate the point, we perform an experiment similar to the discontinuous corotational flow: moving the top wall for a time $\frac{1}{2}T$, and then moving the bottom wall for a time $\frac{1}{2}T$. There is a 5 s pause in between each $\frac{1}{2}T$. The result of this experiment is shown in figure 18(*b*). As expected, folds are generated, and there seem to be two large islands at the top and bottom of the cavity. The islands do not move around the cavity as much as the islands that exist in the previous time-periodic cavity flows. In fact, these two islands stay close to either the top or the bottom of the cavity. This system is much less complicated than the previous cases and might be amenable to some degree of analytical inspection.

It is clear that experiments provide considerable insight into the behaviour of mixing. Results show that islands are nearly inevitable and that they are the major obstruction to mixing. However, the islands can be destroyed by changes in operating conditions, but at the present time we can neither predict these conditions based on theory nor can we predict the approximate sizes of the islands created or the rate of growth of material lines in the chaotic regions. The understanding of all these issues necessitates new theoretical developments and not simply adaptation of existing theory. Undoubtedly, the analysis presented here can be extended; for example, we can focus on the behaviour of horseshoes as done in Chien *et al.* (1986), and many other possibilities and extensions come to mind. However, it seems

unlikely that a complete analysis and understanding of this system can be based on a single viewpoint. Indeed, it seems likely that this experimental system (or similar ones) can serve as a yardstick for the applicability of theoretical concepts pertaining to chaotic mixing in two-dimensional flows.

Could mixing be improved by random forcing? (i.e. a random sequence of top and bottom motions). We have also studied, though not in detail, this situation and a few comments might be in order. First, the number of displacements in the experiments reported here is rather small (order 10; we want produce mixing as fast as possible). Given this small number it is likely that the results will vary widely; some of the sequences lead to poor mixing. Another objection is that random sequence, as opposed to a deterministic sequence, is hard to implement in the context of an engineering design. However, the most important objection is that there are in fact deterministic sequences, which are not periodic, which lead to effective mixing; such sequences are based on a systematic 'destruction' of symmetries (Franjione *et al.* 1989). So far we have not found any sequence which leads to better mixing than those obtained by this method.

The results obtained in terms of passive tracers can be used to launch attacks on more complex situations. The mixing structure obtained by means of passive tracers can be used as a 'fabric' for other processes such as aggregation and breakup (Muzzio & Ottino 1988). Similar experiments to those reported here have been carried out using viscoelastic fluids (e.g. a solution of PAA in glycerine, tracer consisting of dye mixed with the polymer solution) and immiscible fluids (droplets of a low-viscosity fluid in glycerine, droplets mixed with a fluorescent tracer). Other examples can be found in Ottino *et al.* (1988). Undoubtedly, these physical situations are more complicated than the present (base) case. In the viscoelastic case we observe the same general features, such as large-scale folds, except that the regular regions in the viscoelastic fluid are significantly larger than those of the Newtonian case and squeeze out the chaotic regions (Leong 1989). The breakup of droplets in the regular regions is generally less effective than in the chaotic regions and the general structures traced by the fragments of the dispersed fluid correspond closely to those of the passive case. Even though the physics of the base case is not completely understood, the results presented here provide a 'fabric' on which to base the analysis of these more complex situations. However, the richness and complexity of the results obtained indicate that mixing in time-periodic two-dimensional flows is far from being completely understood. In fact, the rather large number of photographs included in this article is a tacit admission of our inability to condense the results further in terms of a few operating rules. We are confident, however, that experimental studies, such as this, can provide a beginning for the understanding of mixing in realistic flow fields.

Finally, a few comments regarding computational prediction might be in order. The remarks of §1 might produce the impression that the computational prediction of our experimental results is impossible. This point should be clarified. Whereas a computational prediction of the exact arrangement of all the striations in the chaotic regions is beyond current capabilities, analyses based on standard finite-difference and finite-element schemes yield remarkably accurate predictions of the coarse structures (i.e. islands and folds) of all the experimental results presented in this work.

We would like to thank John G. Franjione for providing the results given in the Appendix. This work was supported by grants of the National Science Foundation,

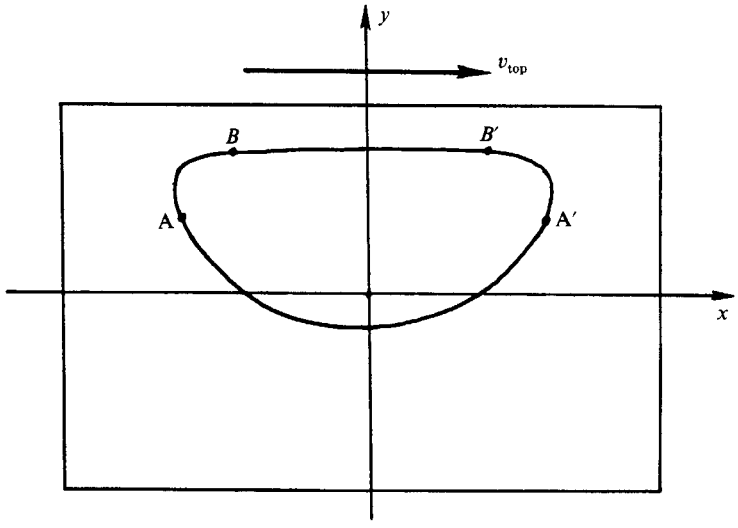

FIGURE 19. Determination of a y-symmetry in a one-wall-moving cavity flow. The closed curve corresponds to a steady-state streamline shown in figure 5 (*a*). Under creeping flow, particle motion from point A to point B due to $\boldsymbol{u}_{top}$ (the velocity field induced in the cavity when the top wall is moved with velocity v_{top}) is equivalent to first reflecting A across the y-axis to A′, followed by a motion $-\boldsymbol{u}_{top}$ (i.e. the inverse motion) from A′ to B′, and then reflecting B′ back across the y-axis to B. This construction is a geometrical demonstration of (A 1), which states that **S** is a symmetry of a map **T** if $\mathbf{T} = \mathbf{S}\mathbf{T}^{-1}\mathbf{S}$.

the Department of Energy, Division of Basic Energy Sciences, and the Materials Research Laboratory of the University of Massachusetts at Amherst.

Appendix. Symmetries in flow fields

The motion due to a time-periodic vector field such as those considered in this paper can in principle be written in the form of a mapping:

$$\boldsymbol{x}_{n+1} = \mathbf{T}(\boldsymbol{x}_n).$$

Here, **T** is a vector transformation which yields the position of a particle at the $(n+1)$th period, given its position at the nth period. A map **T** is said to possess a symmetry if a vector operator **S** can be found such that

$$\mathbf{S}(\mathbf{S}(\boldsymbol{x})) = \boldsymbol{x}, \quad \mathbf{T}(\mathbf{S}(\mathbf{T}(\mathbf{S}(\boldsymbol{x})))) = \boldsymbol{x} \tag{A 1}$$

for all $\boldsymbol{x}$. Often, as is the case with the cavity flow, the explicit mapping is not known. In these cases, symmetry must be deduced through a knowledge of the geometry of the vector field $\boldsymbol{v}(\boldsymbol{x}, t)$. In this case we say that the map possesses a symmetry if the vector field satisfies:

$$\mathbf{S}(-\boldsymbol{v}(\mathbf{S}(\boldsymbol{x}), -t)) = \boldsymbol{v}(\boldsymbol{x}, t)$$

In general, **S** can be orientation-preserving (determinant of the Jacobian of $\mathbf{S} = 1$), in which case the operator **S** is called a *rotational symmetry*, or orientation reversing (determinant of the Jacobian of $\mathbf{S} = -1$), in which case **S** is called a *reflectional symmetry*. Note that the rotation or reflection can be nonlinear (i.e. the Jacobian is not spatially homogeneous). All reflectional symmetries possess a set of fixed points $\{\boldsymbol{x}\}$ (i.e. $\mathbf{S}(\boldsymbol{x}) = \boldsymbol{x}$) which compose the *fixed line* of the symmetry. Near the fixed line, the symmetry operator acts as a reflection across the line.

Since the cavity flow is operated in the Stokes regime and the governing equations are linear, the overall velocity field can be expressed as a linear combination of the velocities due to the motion of the top and bottom cavity walls:

$$\boldsymbol{v}(\boldsymbol{x},t) = v_{\text{top}}(t)\,\boldsymbol{u}_{\text{top}}(\boldsymbol{x}) + v_{\text{bot}}(t)\,\boldsymbol{u}_{\text{bot}}(\boldsymbol{x}). \tag{A 2}$$

Here, $\boldsymbol{u}_{\text{top}}$ and $\boldsymbol{u}_{\text{bot}}$ are the velocity fields that are induced owing to the steady motion of the top and bottom walls only. The streamline patterns of these steady flows are shown in figure 5. The symmetries of the motion can easily be deduced from the geometry of the streamlines.

Consider a Cartesian coordinate system with the origin located at the centre of the cavity (figure 19). Since the flow occurs in the Stokes regime, the motion due to either $\boldsymbol{u}_{\text{top}}$ or $\boldsymbol{u}_{\text{bot}}$ is symmetric with respect to reflections about the y-axis, which is denoted as $\mathbf{S}_y$, and given by

$$\mathbf{S}_y : (x_1, x_2) \rightarrow (-x_1, x_2)$$

For example, consider the motion due to $\boldsymbol{u}_{\text{top}}$ (see figure 19). Particle motion from point A to point B due to $\boldsymbol{u}_{\text{top}}$ is equivalent to first reflecting A across the y-axis to A′, motion due to $-\boldsymbol{u}_{\text{top}}$ (i.e. the inverse motion) from A′ to B′, and then reflecting B′ back across the y-axis to B. This construction is a geometrical demonstration of (A 1), which states that $\mathbf{S}$ is a symmetry of a map $\mathbf{T}$ if $\mathbf{T} = \mathbf{S}\mathbf{T}^{-1}\mathbf{S}$.

Now, both $\boldsymbol{u}_{\text{top}}$ and $\boldsymbol{u}_{\text{bot}}$ are symmetric with respect to reflections about the y-axis; that is

$$\mathbf{S}_y(-\boldsymbol{u}_{\text{top}}(\mathbf{S}_y(\boldsymbol{x}))) = \boldsymbol{u}_{\text{top}}(\boldsymbol{x}), \quad \mathbf{S}_y(-\boldsymbol{u}_{\text{bot}}(\mathbf{S}_y(\boldsymbol{x}))) = \boldsymbol{u}_{\text{bot}}(\boldsymbol{x}).$$

Substituting this relation into (A 2), we obtain

$$\begin{aligned}\boldsymbol{v}(\boldsymbol{x},t) &= v_{\text{top}}(t)\,\mathbf{S}_y(-\boldsymbol{u}_{\text{top}}(\mathbf{S}_y(\boldsymbol{x}))) + v_{\text{bot}}(t)\,\mathbf{S}_y(-\boldsymbol{u}_{\text{bot}}(\mathbf{S}_y(\boldsymbol{x}))) \\ &= \mathbf{S}_y(-\boldsymbol{v}(\mathbf{S}_y(\boldsymbol{x}),t)).\end{aligned}$$

Thus, $\mathbf{S}_y$ will be a symmetry of the time-dependent flow if

$$v_{\text{top}}(t) = v_{\text{top}}(-t), \quad v_{\text{bot}}(t) = v_{\text{bot}}(-t).$$

This can equivalently be stated as

$$v_{\text{top}}(t-\tfrac{1}{2}T) = v_{\text{top}}(\tfrac{1}{2}T-t), \quad v_{\text{bot}}(t-\tfrac{1}{2}T)) = v_{\text{bot}}(\tfrac{1}{2}T-t).$$

That is, both waveforms are even functions about the half-period.

REFERENCES

Allègre, C. J. & Turcotte, D. L. 1986 Implication of a two-component marble-cake mantle. *Nature* **323**, 123–127.

Aref, H. 1984 Stirring by chaotic advection. *J. Fluid Mech.* **143**, 1–21.

Aref, H. & Balachandar, S. 1986 Chaotic advection in a Stokes flow. *Phys. Fluids* **29**, 3515–3521.

Chaiken, J., Chevray, R., Tabor, M. & Tan, Q. M. 1986 Experimental study of Lagrangian turbulence in a Stokes flow. *Proc. R. Soc. Lond.* A **408**, 165–174.

Chien, W. L., Rising, H. & Ottino, J. M. 1986 Laminar mixing and chaotic mixing in several cavity flows. *J. Fluid Mech.* **170**, 419–451.

Doherty, M. F. & Ottino, J. M. 1988 Chaos in deterministic systems: strange attractors, turbulence and applications in chemical engineering. *Chem. Engng Sci.* **43**, 139–183.

Franjione, J. G., Leong, C. W. & Ottino, J. M. 1989 Symmetries within chaos: a route to effective mixing. *Phys. Fluids* A to appear.

Franjione, J. G. & Ottino, J. M. 1987 Feasibility of numerical tracking of material lines and surfaces in chaotic flows. *Phys. Fluids* **30**, 3641–3643.

GREENE, J. M., MACKAY, R. S., VIVALDI, F. & FEIGENBAUM, M. J. 1981 Universal behaviour in families of area preserving maps. *Physica* **D3**, 468–486.

GUCKENHEIMER, J. & HOLMES, P. 1983 *Nonlinear Oscillations, Dynamical Systems, and Bifurcations of Vectors Fields*. Springer.

KHAKHAR, D. V., RISING, H. & OTTINO, J. M. 1986 An analysis of chaotic mixing in two model flows. *J. Fluid Mech.* **172**, 419–451.

LEONG, C. W. 1989 A detailed analysis of chaotic mixing of viscous fluids in time-periodic cavity flows. Ph.D. thesis University of Massachusetts, Amherst.

MIDDLEMAN, S. 1977 *Fundamentals of Polymer Processing*. McGraw-Hill.

MUZZIO, F. J. & OTTINO, J. M. 1988 Coagulation in chaotic flows. *Phys. Rev.* A **38**, 2516–2524.

OTTINO, J. M. 1989*a* *The Kinematics of Mixing: Stretching, Chaos, and Transport*. Cambridge University Press.

OTTINO, J. M. 1989*b* The mixing of fluids. *Sci. Am.* **260**, 56–67.

OTTINO, J. M. & CHELLA, R. 1983 Mixing of polymeric liquids: a brief review and recent theoretical developments. *Polym. Engng Sci.* **23**, 165–176.

OTTINO, J. M., LEONG, C. W., RISING, H. & SWANSON, P. 1988 Morphological structures produced by mixing in chaotic flows. *Nature* **333**, 419–425.

SWANSON, P. D. & OTTINO, J. M. 1990 A comparative computational and experimental study of chaotic mixing of viscous fluids. *J. Fluid Mech.* (to appear).

WEIJERMARS, R. 1988 Convection experiments in high Prandtl number silicones. Part 2. Deformation, displacement and mixing in the Earth's mantle. *Tectonophys.* **154**, 97–123.